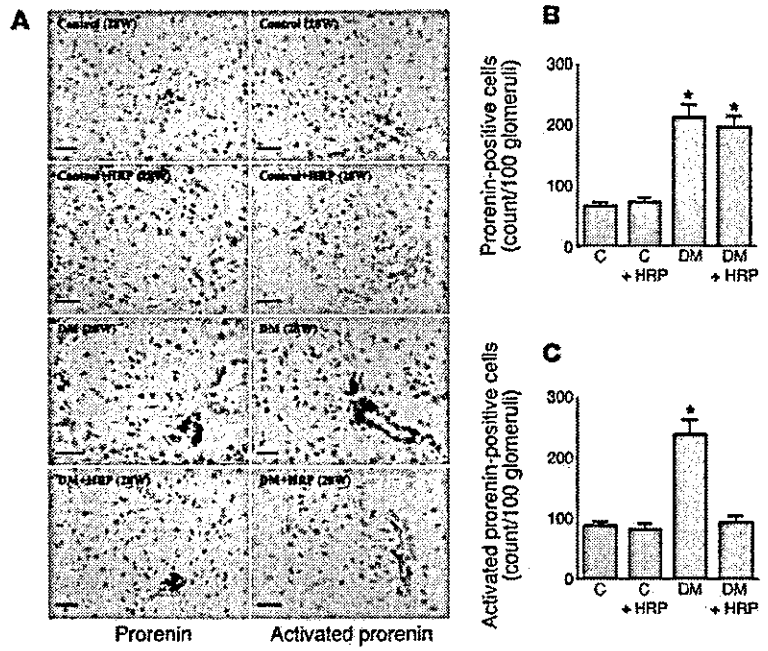

Figure 8
Kidney levels of total prorenin and activated prorenin in C rats ($n = 6$), C + HRP rats ($n = 6$), DM rats ($n = 6$), and DM + HRP rats ($n = 6$) at 28 weeks of age. **(A)** Immunohistochemistry of prorenin and active center of renin that indicates total prorenin and activated prorenin, respectively. The photomicrographs show increases in both total prorenin and activated prorenin at the juxtaglomerular area of diabetic rat kidneys. HRP treatment did not alter the increased staining of total prorenin but inhibited the enhanced staining of activated prorenin. Scale bars: 25 μm. **(B)** Quantitative analysis of prorenin-positive cells in a juxtaglomerular area. The graph shows an increase in prorenin-positive cells in DM and DM + HRP rats. **(C)** Quantitative analysis of activated prorenin in a juxtaglomerular area. The graph shows an increase in activated prorenin in DM and its inhibition by HRP treatment. *$P < 0.05$ versus C rats.

However, since high extracellular glucose stimulates the synthesis of angiotensinogen in a concentration-dependent manner in rat proximal tubular cells (20), the present study cannot exclude the possibility that angiotensinogen synthesis regionally increases in the proximal tubule (13, 21) or even in the glomerulus. Previous studies showed that kidney renin mRNA levels increased at the early onset of diabetes in spontaneously or streptozotocin-induced diabetic rats (13, 17, 19, 21) and decreased markedly thereafter (17). The present study demonstrated that both the total kidney renin (proteolytically activated and prorenin) content and kidney renin mRNA level were lower in the DM rats than in the C rats at 12 and 20 weeks of age (8 and 16 weeks of diabetes) when the nephropathy develops, and they were similar at 28 weeks of age (24 weeks of diabetes) when the nephropathy progresses. HRP administration did not alter total kidney renin content or kidney renin mRNA levels in either control or diabetic rats at any age or length of diabetes (Figure 6C and 7A). Thus, the total amount of intrarenal renin and prorenin generated in the kidneys may be decreased during the development of diabetic nephropathy. The total activity of renin and prorenin did increase in the kidneys of diabetic rats, however, because the result of the present study showed the increased staining of the exposed active center of renin/prorenin in the kidneys of diabetic rats and its inhibition by HRP. Previous studies also demonstrated increased ability of the kidney to generate Ang I in diabetic rats, which was called "renal renin concentration" (21). Taken together, during the development of diabetic nephropathy, the kidneys of diabetic rats increased levels of Ang I and II without any changes in renin, ACE, or angiotensinogen synthesis, and continuous infusion of HRP completely inhibited the increased kidney levels of Ang I and II without affecting the kidney levels of renin, ACE, or angiotensinogen mRNA. These results suggest that intrarenal renin activity increases during the development of diabetic nephropathy and that nonproteolytic activation of prorenin significantly contributes to the increased intrarenal renin activity.

The reason why the nonproteolytic activation of prorenin occurs in diabetic organ remains unclear. We believe, however, that the present studies provide a credible explanation. Consistent with previous in vitro and in vivo studies (22, 23), the kidney cathepsin B mRNA levels significantly decreased during the development of diabetic nephropathy (Figure 7D). This result suggests that the decreased prorenin processing can increase the ratio of prorenin to renin in diabetic rat kidneys. In fact, the immunohistochemical staining of prorenin significantly increased in diabetic rat kidneys compared with control rat kidneys (Figure 8, A and B), although total renin content of diabetic rat kidneys was similar to or lower than that of control rat kidneys (Figure 6C). Since both renin and prorenin competitively bind to a renin/prorenin receptor (9), the relative increase in prorenin versus renin could cause more binding of prorenin to its receptor, leading to the nonproteolytic activation of prorenin. This idea was supported by the result of the present study showing that the inhibition of nonproteolytic activation of prorenin by HRP significantly suppresses the increased immunohistochemical staining of exposed active center of renin/prorenin in the kidneys of diabetic rats (Figure 8, A and C). Alternatively, nonproteolytic prorenin-activators, such as a renin/prorenin receptor (9), or their affinity to prorenin might be increased in diabetic organ. Further studies will be needed to determine the reason why the nonproteolytic activation of prorenin occurs in the diabetic organ.

In conclusion, even though diabetic animals have high plasma prorenin levels and low plasma renin levels, suggesting a suppressed circulating RAS (1), Ang II type 1 receptor blockers have a beneficial effect in preventing the development and progression of diabetic organ damage (24, 25). This study clearly demonstrated that the development of diabetic nephropathy is associated with the activated kidney RAS and suggested that nonproteolytic activation of prorenin significantly contributes to the activation of the kidney RAS and the development of diabetic nephropathy.

Therefore, we propose that substances that inhibit nonproteolytic activation of prorenin, such as HRP, is useful in drug therapy strategies to prevent diabetic organ damage.

Methods

Preparation of rat prorenin handle peptide and its Ab. Figure 1 shows the prosegment of rat prorenin. To cover the handle region (position 11–15) (5), we designed a decapeptide, NH_2-RILLKKMPSV-COOH, as an HRP of rat prorenin and purified it by HPLC on a C-18 reverse-phase column. The purity and retention time of HPLC were 97.6% and 26.2 minutes, respectively. The mass of the product was 1,185.7, similar to the theoretical mass value (1,186.0). Anti-rat HRP Ab was raised against a peptide, RILLKK-MPSVC, conjugated with keyhole limpet hemocyanin in rabbits. HRP was used for determining the titer of the antiserum using a Vectastatin ABC-AP rabbit IgG kit (Vector Laboratories) and as the ligand of an affinity column for purification of the Ab. High-titer antisera were obtained 6 weeks after the first immunization. The affinity gel was prepared by conjugation of Biogel 102 (amine-coupled gel; Bio-Rad Laboratories) through a cysteine residue of antigen peptide as a ligand. The Ab was purified with the affinity column, and the concentration of the purified Ab (3.90 mg/ml) was calculated using an extinction coefficient of 1.35 at 1 mg/ml IgG and 280 nm.

Immunoblot analysis. The recombinant rat prorenin and renin was subjected to 12% SDS-PAGE and electrophoretically transferred to the polyvinylidene difluoride membrane. Renin was prepared by the trypsin treatment of prorenin; that is, prorenin was incubated with 200 μg/ml of trypsin for 20 minutes at pH 7.4 and 25°C, and then the trypsin action was arrested with 1 mM PMSF. The membrane was incubated separately with rabbit anti-rat renin antiserum (1:1,000) (26) and 3 nM purified rabbit anti-handle region peptide Ab for 1 hour at room temperature in the absence or presence of 10, 100, and 1,000 nM regional peptides of prorenin prosegment. After being washed, the immunocomplex on these sheets was visualized using horseradish peroxidase–conjugated secondary anti-rabbit IgG and diaminobenzidine.

Animals. We maintained male Sprague-Dawley rats (Charles River Laboratories Inc.) in a temperature-controlled room that was maintained at 23°C and a 12-hour light/12-hour dark cycle, with free access to water and a normal-salt diet rat chow (0.4% NaCl) (CE-2; Nihon Clea). The Keio University Animal Care and Use Committee approved all experimental protocols. At 3 weeks of age, under sodium pentobarbital (50 mg/kg i.p.) anesthesia, we removed the left kidney of 100- to 150-g rats and divided the heminephrectomized rats into four groups: the C, C + HRP, DM, and DM + HRP groups. Diabetic rats received i.p. 10 mM citrate buffer with 65 mg/kg of streptozotocin (Wako Pure Chemical), and nondiabetic control rats received 10 mM citrate buffer alone, at 4 weeks of age. Every 28 days we changed the subcutaneously implanted osmotic minipump (model 2004, for 28-day use; Alzet Osmotic Pumps) containing saline or a HRP (0.1 mg/kg), and we decapitated six rats at 12, 20, and 28 weeks of age to obtain the blood and right kidney of each animal. In our preliminary study, an osmotic minipump with a NH_2-SFGR-COOH (0.1 mg/kg, $n = 3$) or NH_2-MTRI-SAE-COOH (0.1 mg/kg, $n = 3$) was also implanted in diabetic rats. These peptides, however, did not inhibit the development of glomerulosclerosis or increase in the levels of Ang I and II in the kidneys of diabetic rats.

Experiments. We measured the systolic arterial BP of the rats at 4, 8, 12, 16, 20, 24, and 28 weeks of age by tail-cuff plethysmography. The 24-hour urine was collected in a metabolic cage, and urinary protein excretion and creatinine were determined with a Micro TP test kit (Wako Pure Chemical) and a creatinine HA test kit (Wako Pure Chemical), respectively. Blood was obtained from the tail vein, and glucose was analyzed with a glucose C test kit (Wako Pure Chemical).

Morphological and immunohistochemical evaluation. A part of the kidney removed from each animal was fixed in 10% formalin in phosphate buffer (pH 7.4). Paraffin-embedded sections were stained by the PAS method. We quantitatively determined the total area of sclerosis within the glomerular tuft, adopting the semiquantitative scoring system proposed by El-Nahas, et al. (27). A glomerulosclerosis index was derived for each animal by examining 100 glomeruli at ×400 magnification. The severity of glomerulosclerosis was expressed on an arbitrary scale from 0 to 4: grade 0, normal glomeruli; grade 1, presence of mesangial expansion/thickening of the basement membrane; grade 2, mild to moderate segmental hyalinosis/sclerosis involving less than 50% of the glomerular tuft; grade 3, diffuse glomerular hyalinosis/sclerosis involving more than 50% of the tuft; grade 4, diffuse glomerulosclerosis with total tuft obliteration and collapse. The resulting index in each animal was expressed as a mean of all scores obtained.

For immunohistochemical staining, deparaffinized sections were pretreated with proteinase K, the sections were then boiled in citrate buffer with microwaves to unmask antigenic sites, and endogenous biotin was blocked with a biotin-blocking system (X0590; DAKO Corp.). Next, the sections were immersed in 3% H_2O_2 in methanol to inhibit endogenous peroxidase and then precoated with 1% nonfat milk in PBS to block nonspecific binding. For immunohistochemical staining of type IV collagen and prorenin, a cocktail of rabbit polyclonal Abs to the anti-a2(IV), -a4(IV), and -a5(IV) chains of type IV collagen (1:400; a generous gift of R. Kalluri, Center for Matrix Biology, Beth Israel Deaconess Medical Center) (28) and the rabbit anti-rat HRP Ab were applied, respectively, to the sections as the primary Ab. The sections were incubated with a biotin-conjugated anti-rabbit IgG as the secondary Ab. For immunohistochemical staining of the exposed active center of renin, a goat polyclonal Ab to rat renin that crossreacts with nonproteolytically activated prorenin but not with natural prorenin (1:1,000) (26, 29, 30) was applied to the sections as the primary Ab. The sections were incubated with a biotin-conjugated anti-goat IgG as the secondary Ab. The Ab reactions were visualized by using a VectaStain ABC Standard Kit (Vector Laboratories) and an AEC standard kit (DAKO Corp.) according to the manufacturers' instructions. We quantitatively determined the immunoreactive type IV collagen-positive area in each glomerulus at ×200 magnification with a Mac SCOPE (version 2.5; Mitani Corp.) and expressed it as a percentage of the whole cross-sectional area of the glomerulus. The levels of prorenin and the exposed active center of renin were evaluated by counting the number of juxtaglomerular cells where the signal intensity of the reaction products was above the visible level. The final overall score was calculated as the means of the values for 100 glomeruli per group of rats.

Measurements of renin and Ang peptides. Immediately after decapitation, a 3-ml blood specimen was collected into a tube containing 30 μl of EDTA (500 mM), 15 μl of enalaprilat (1 mM), and 30 μl of *o*-phenanthroline (24.8 mg/ml) and pepstatin (0.2 mM), and plasma samples were obtained by centrifugation. Plasma renin activity was determined with a RIA coated bead kit (Dinabott Radioisotope Institute). Plasma prorenin level was calculated by subtracting plasma renin activity from plasma total (inactive plus active) renin activity, as described previously (31). For the measurement of kidney total renin content, a part of the removed kidney was weighed, placed in 5 ml of buffer containing 2.6 mM EDTA, 1.6 mM dimercaprol, 3.4 mM 8-hydroxyquinoline sulfate, 0.2 mM PMSF, and 5 mM ammonium acetate, homogenized with a chilled glass homogenizer, and then centrifuged. The renin activity of the supernatant was determined as described previously (32). For the determination of kidney Ang I and II content, half of the removed kidney was weighed, placed in ice-cold methanol (10% wt/vol), homogenized with a chilled glass homogenizer, and then centrifuged. The supernatant was then dried and reconstituted in 4 ml of 50 mM sodium phosphate buffer containing 1% albumin. Plasma and reconstituted samples from the kidneys were extracted with a Bond-Elut column (Analytichem Co.), and the eluents were evaporated to dryness and reconstituted in Ang peptide assay diluent. The Ang I and II content was quantitatively

determined by RIA using rabbit anti-Ang I antiserum and rabbit anti-Ang II antiserum (Amel Inc.) as previously reported (33).

Real-time quantitative RT-PCR analysis. We extracted total RNA from part of the kidney removed from each animal by using an RNeasy Mini Kit (QIAGEN KK) and performed a real-time quantitative RT-PCR by using the TaqMan One-Step RT-PCR Master Mix Reagents Kit with an ABI Prism 7700 HT Detection System (Applied Biosystems Inc.) and probes and primers for the rat genes encoding the following: renin (forward, 5′-GCTACATGGAGAATGGGACTGAA-3′; reverse, 5′-ACCACATCTTGGCTGAGGAAAC-3′; probe, 5′-FAM-CCATCCACTATGGATCAGGGAAGGTCAA-TAMRA-3′); ACE (forward, 5′-CTGCCTCCCAACGAGTTAGAA-3′; reverse, 5′-CGGGACGTGGCCATTATATT-3′; probe, 5′-FAM-AAATGGCACTTGTCTGTCACTGGAGCCTAMRA-3′); angiotensinogen (forward, 5′-AGCACGGACAGCACCCTATT-3′; reverse, 5′-AGAACTCATGGAGCCCAGTCA-3′; probe, 5′-FAM-TCAACACCTACGTTCACTTCCAAGGGAAGA-TAMRA-3′); cathepsin B (forward, 5′-AAATCAGGCGTATACAAGCATGA-3′; reverse, 5′-GCCCAGAATGCGGATGG-3′; probe, 5′-FAM-CCGGTGATGTGATGGGAGGCCA-TAMRA-3′); and GAPDH (forward, 5′-TGACAACTCCCTCAAGATTGTCA-3′; reverse, 5′-GGCATGGACTGTGGTCATGA-3′; probe, 5′-FAM-TGCATCCTGCACCACCAACTGCTTAG-TAMRA-3′); as described previously (34, 35).

Statistical analyses. Within-group statistical comparisons were made by one-way ANOVA for repeated measures followed by the Newman-Keuls post hoc test. Differences between two groups were evaluated by two-way ANOVA for repeated measures combined with the Newman-Keuls post-hoc test. A P value of less than 0.05 was considered significant. Data are reported as means ± SEM.

Acknowledgments

This work was supported in part by grants 14571073, 1503340, and 16613002 from the Ministry of Education, Science, and Culture of Japan; a grant from the Takeda Science Foundation (to A. Ichihara); NIH research grant HL-58205; and Health and Labour Sciences Research Grants, Research on Measures for Intractable Diseases, from the Ministry of Health, Labour, and Welfare of Japan. We thank Rika Wakita for her dedicated attention to the many details involved in the preparation of this paper.

Received for publication February 23, 2004, and accepted in revised form August 24, 2004.

Address correspondence to: Atsuhiro Ichihara, Department of Internal Medicine, Keio University School of Medicine, 35 Shinanomachi, Shinjuku-ku, Tokyo, 160-8582, Japan. Phone: 81-3-5363-3796; Fax: 81-3-3359-2745; E-mail: atzichi@sc.itc.keio.ac.jp.

1. Luetscher, J.A., Kraemer, F.B., Wilson, D.M., Schwartz, H.C., and Bryer-Ash, M. 1985. Increased plasma inactive renin in diabetes mellitus: a marker of microvascular complications. *N. Engl. J. Med.* 312:1412–1417.
2. Deinum, J., et al. 1999. Increase in serum prorenin precedes onset of microalbuminuria in patients with insulin-dependent diabetes mellitus. *Diabetologia.* 42:1006–1010.
3. Véniant, M., et al. 1996. Vascular damage without hypertension in transgenic rats expressing prorenin exclusively in the liver. *J. Clin. Invest.* 98:1966–1970.
4. Peters, J., et al. 2002. Functional significance of prorenin internalization in the rat heart. *Circ. Res.* 90:1135–1141.
5. Suzuki, F., et al. 2003. Human prorenin has "gate and handle" regions for its non-proteolytic activation. *J. Biol. Chem.* 278:22217–22222.
6. Maru, I., Ohta, Y., Murata, K., and Tsukada, Y. 1996. Molecular cloning and identification of N-acyl-D-glucosamine 2-epimerase from porcine kidney as a renin-binding protein. *J. Biol. Chem.* 271:16294–16299.
7. Van-Kesteren, C.A.M., et al. 1997. Mannose 6-phosphate receptor-mediated internalization and activation of prorenin by cardiac cells. *Hypertension.* 30:1389–1396.
8. Admiraal, P.J.J., et al. 1999. Uptake and proteolytic activation of prorenin by cultured human endothelial cells. *J. Hypertens.* 17:621–629.
9. Nguyen, G., et al. 2002. Pivotal role of the renin/prorenin receptor in angiotensin II production and cellular responses to renin. *J. Clin. Invest.* 109:1417–1427. doi:10.1172/JCI200214276.
10. deCavanagh, E.M.V., et al. 2001. Enalapril attenuates oxidative stress in diabetic rats. *Hypertension.* 38:1130–1136.
11. Onozato, M.L., Tojo, A., Goto, A., Fujita, T., and Wilcox, C.S. 2002. Oxidative stress and nitric oxide synthase in rat diabetic nephropathy: effects of ACEI and ARB. *Kidney Int.* 61:186–194.
12. Hayashi, M., Senba, S., Saito, I., Kitajima, W., and Saruta, T. 1983. Changes in blood pressure, urinary kallikrein, and urinary prostaglandin E2 in rats with streptozotocin-induced diabetes. *Naunyn Schmiedebergs Arch. Pharmacol.* 322:290–294.
13. Zimpelmann, J., et al. 2000. Early diabetes mellitus stimulates proximal tubule renin mRNA expression in the rat. *Kidney Int.* 58:2320–2330.
14. Vallon, V., Wead, L.M., and Blantz, R.C. 1995. Renal hemodynamics and plasma and kidney angiotensin II in established diabetes mellitus in rats: effect of sodium and salt restriction. *J. Am. Soc. Nephrol.* 5:1761–1767.
15. Kennefick, T.M., Oyama, T.T., Thompson, M.M., Vora, J.P., and Anderson, S. 1996. Enhanced renal sensitivity to angiotensin actionc in diabetes mellitus in the rat. *Am. J. Physiol.* 271:F595–F602.
16. Campbell, D.J., Kelly, D.J., Wilkinson-Berka, J.L., Cooper, M.E., and Skinner, S.L. 1999. Increased bradykinin and "normal" angiotensin peptide levels in diabetic Sprague-Dawley and transgenic (mRen-2)27 rats. *Kidney Int.* 56:211–221.
17. Everett, A.D., et al. 1992. Renin and angiotensinogen expression during the evolution of diabetes. *Hypertension.* 19:70–78.
18. Kalinyak, J.E., et al. 1993. The renin-angiotensin system in streptozotocin-induced diabetes mellitus in the rat. *J. Am. Soc. Nephrol.* 4:1337–1345.
19. Choi, K.C., et al. 1997. Alterations of intrarenal renin-angiotensin and nitric oxide systems in streptozotocin-induced diabetic rats. *Kidney Int.* 52(Suppl.):S23–S27.
20. Zhang, S.-L., et al. 1999. Molecular mechanisms of glucose action on angiotensinogen gene expression in rat proximal tubular cells. *Kidney Int.* 55:454–464.
21. Anderson, S., Jung, F.F., and Ingelfinger, J.R. 1993. Renal renin-angiotensin system in diabetes: functional, immunohistochemical, and molecular biological correlations. *Am. J. Physiol.* 265:F477–F486.
22. Leehey, D.J., Song, R.H., Alavi, N., and Singh, A.K. 1995. Decreased degradative enzymes in mesangial cells cultured in high glucose media. *Diabetes.* 44:929–935.
23. Song, R.H., Singh, A.K., and Leehey, D.J. 1999. Decreased glomerular proteinase activity in the streptozotocin diabetic rat. *Am. J. Nephrol.* 19:441–446.
24. Lewis, E.J., et al. 2001. Renoprotective effect of the angiotensin-receptor antagonist irbesartan in patients with nephropathy due to type 2 diabetes. *N. Engl. J. Med.* 345:851–860.
25. Brenner, B.M., et al. 2001. Effects of losartan on renal and cardiovascular outcomes in patients with type 2 diabetes and nephropathy. *N. Engl. J. Med.* 345:861–869.
26. Takii, Y., Figueiredo, A.F.S., and Inagami, T. 1985. Application of immunochemical methods to the identification and characterization of rat kidney inactive renin. *Hypertension.* 7:236–243.
27. El-Nahas, A.M., Bassett, A.H., Cope, G.H., and Carpentier, J.E. 1991. Role of growth hormone in the development of experimental renal scarring. *Kidney Int.* 40:29–34.
28. Kalluri, R., Shield, C.F., Todd, P., Hudson, B.G., and Neilson, E.G. 1997. Isoform switching of type IV collagen is developmentally arrested in X-linked Alport syndrome leading to increased susceptibility of renal basement membranes to endoproteolysis. *J. Clin. Invest.* 99:2470–2478.
29. Inagami, T., Murakami, T., Higuchi, K., and Nakajo, S. 1991. Roles of renal and vascular renin in spontaneous hypertension and switching of the mechanism upon nephrectomy. *Am. J. Hypertens.* 4:15S–22S.
30. Iwai, N., Inagami, T., Ohmichi, N., and Kinoshita, M. 1996. Renin is expressed in rat macrophage/monocyte cells. *Hypertension.* 27:399–403.
31. Hirota, N., Ichihara, A., Koura, Y., Hayashi, M., and Saruta, T. 2002. Phospholipase D contributes to transmural pressure control of prorenin processing in juxtaglomerular cell. *Hypertension.* 39:363–367.
32. Kobori, H., et al. 1997. Thyroid hormone stimulates renin synthesis in rats without involving the sympathetic nervous system. *Am. J. Physiol.* 272:E227–E232.
33. Nishiyama, A., Seth, D.M., and Navar, L.G. 2002. Renal interstitial fluid angiotensin I and angiotensin II concentrations during local angiotensin-converting enzyme inhibition. *J. Am. Soc. Nephrol.* 13:2207–2212.
34. Naito, Y., Tsujino, T., Fujioka, Y., Ohyanagi, M., and Iwasaki, T. 2002. Augmented diurnal variations of the cardiac renin-angiotensin system in hypertensive rats. *Hypertension.* 40:827–833.
35. Wasselius, J., Wallin, H., Abrahamson, M., and Ehinger, B. 2003. Cathepsin B in the rat eye. *Graefe's Arch. Clin. Exp. Ophthalmol.* 241:934–942.

ELSEVIER

Mechanisms of Development 121 (2004) 547–557

www.elsevier.com/locate/modo

Identification of kidney mesenchymal genes by a combination of microarray analysis and *Sall1-GFP* knockin mice☆

Minoru Takasato[a,b], Kenji Osafune[a,c], Yuko Matsumoto[a], Yuki Kataoka[d], Nobuaki Yoshida[d], Hiroko Meguro[e], Hiroyuki Aburatani[e], Makoto Asashima[b,c], Ryuichi Nishinakamura[a,f,g,*]

[a]*Division of Stem Cell Regulation, The Institute of Medical Science, The University of Tokyo, 4-6-1 Minato-ku Shirokanedai, Tokyo 108-8639, Japan*
[b]*Department of Biological Sciences, Graduate School of Science, The University of Tokyo, Tokyo 113-8654, Japan*
[c]*Department of Life Sciences (Biology), Graduate School of Art and Sciences, The University of Tokyo, Tokyo 153-8902, Japan*
[d]*Laboratory of Gene Expression and Regulation, The Institute of Medical Science, The University of Tokyo, Tokyo 108-8639, Japan*
[e]*Genome Science Division, Research Center for Advanced Science and Technology, The University of Tokyo, Tokyo 153-8904, Japan*
[f]*Division of Integrative Cell Biology, Institute of Molecular Embryology and Genetics, Kumamoto University, Kumamoto 860-0811, Japan*
[g]*PREST, JST, Saitama 332-0012, Japan*

Received 7 November 2003; received in revised form 8 March 2004; accepted 7 April 2004

Available online 22 April 2004

Abstract

SALL1, a causative gene for Townes-Brocks syndrome, encodes a zinc finger protein, and its mouse homolog (*Sall1*) is essential for metanephros development, as noted during gene targeting. In the embryonic kidney, *Sall1* is expressed abundantly in mesenchyme-derived structures from condensed mesenchyme, S-, comma-shaped bodies, to renal tubules and podocytes. We generated mice in which a green fluorescent protein (*GFP*) gene was inserted into the *Sall1* locus and we isolated the *GFP*-positive population from embryonic kidneys of these mice by fluorescein-activated cell sorting. The *GFP*-positive population indeed expressed mesenchymal genes, while the negative population expressed genes in the ureteric bud. To systematically search for genes expressed in the mesenchyme-derived cells, we compared gene expression profiles in the *GFP*-positive and -negative populations using microarray analysis, followed by in situ hybridization. We detected many genes known to be important for metanephros development including *Sall1, GDNF, Raldh2, Pax8* and *FoxD1*, and genes expressed abundantly in the metanephric mesenchyme such as *Unc4.1, Six2, Osr-2* and *PDGFc*. We also found groups of genes including *SSB-4, Smarcd3, μ-Crystallin, TRB-2*, which are not known to be expressed in the metanephric mesenchyme. Therefore a combination of microarray technology and *Sall1-GFP* mice is useful for systematic identification of genes expressed in the developing kidney.

Keywords: Kidney development; Microarray; *Sall1*; Knockin; Fluorescein-activated cell sorting; Metanephric mesenchyme

1. Introduction

In the mammalian kidney there are stromal cells, glomeruli, proximal and distal tubules, loops of Henle and collecting ducts, but all these components originate from only two types of tissues, epithelium of the ureteric bud and the metanephric mesenchyme. Around E11 in mice, the metanephric mesenchyme induces the ureteric bud to invade the metanephric mesenchyme and branch. Upon reciprocal induction by the ureteric bud, the mesenchymal cells aggregate and form blastema around the ureteric bud. The blastema develops into epithelial cells that form the nephron. The region of the metanephric mesenchyme diminishes gradually until 7 days after birth, and kidney development is complete when the metanephric mesenchyme disappears. Metanephric mesenchymal cells differentiate into at least three distinct cell types; glomerular, proximal and distal tubule epithelia as noted in retroviral mediated *lac-Z* gene transfer assay (Herzlinger et al., 1992), demonstrating that the metanephric mesenchyme represents multipotent progenitor cells of the nephron.

☆ Supplementary data associated with this article can be found, in the online version, at doi = 10.1016/j.mod.2004.04.007.

* Corresponding author. Address: Division of Integrative Cell Biology, Institute of Molecular Embryology and Genetics, Kumamoto University, 2-2-1 Honjo, Kumamoto 860-0811, Japan. Tel.: +81-96-373-6615; fax: +81-96-373-6618.

E-mail address: ryuichi@kaiju.medic.kumamoto-u.ac.jp (R. Nishinakamura).

0925-4773/$ - see front matter © 2004 Elsevier Ireland Ltd. All rights reserved.
doi:10.1016/j.mod.2004.04.007

Molecular mechanisms of kidney development have been determined mostly by gene targeting, and many mesenchymal genes including *WT1*, *Eya1*, *GDNF* and *Six1* are known to have important roles in kidney development. The transcription factor *WT1* is first expressed in the metanephric mesenchyme before induction, and in *WT1* null mutant mice the ureter never reaches the mesenchyme and consequently the mesenchyme undergoes apoptosis (Kreidberg et al., 1993). The transcriptional coactivator *Eya1* is only expressed in the metanephric mesenchyme and *Eya1* $-/-$ mice show renal agenesis and their posterior intermediate mesoderm fails to produce the glial-derived neurotrophic factor (*GDNF*) (Xu et al., 1999; Buller et al., 2001). *GDNF* has been identified as a mesenchyme-derived signal that acts on the receptor tyrosine kinase (*Ret*) and *Gfrα1* coreceptor which are distributed in the ureteric epithelium and induces it to produce a ureteric bud which invades the metanephric mesenchyme (Sainio et al., 1997). Indeed, the null mutants of *GDNF*, *Ret* and *Gfrα1* show a similar perturbation of ureteric bud outgrowth (Schuchardt et al., 1994; Moore et al., 1996; Pichel et al., 1996; Sanchez et al., 1996; Cacalano et al., 1998). The homeodomain transcriptional factor *Six1* is expressed in the metanephric mesenchyme before and after induction, and *Six1*-knockout mice lack kidneys because of a failure of metanephric induction (Xu et al., 2003).

Sall1 is also expressed in the metanephric mesenchyme prior to bud invasion and continues in the induced condensing mesenchyme around ureteric bud tips and cells of mesenchymal origin. *Sall1* is the mouse homologue of *Drosophila sal* that is the region-specific homeotic gene characterized by unique multiple double zinc finger motifs (Kuhnlein et al., 1994). Humans and mice have at least four *sal*-related genes, respectively (*SALL1*, *-2*, *-3* and *-4* for humans and *Sall1*, *-2*, *-3* and *-4* for mice) (Kohlhase et al., 1996, 1999, 2000, 2002). *SALL1* is located on chromosome 16q12.1, and heterozygous mutations of *SALL1* lead to Townes-Brocks syndrome, an autosomal-dominant disease with features of dysplastic ears, preaxial polydactyly, imperforate anus and, less commonly, kidney and heart anomalies (Kohlhase et al., 1998). Mice deficient in *Sall1* die in the perinatal period, and kidney agenesis or severe dysgenesis are present (Nishinakamura et al., 2001). Homozygous deletion of *Sall1* results in an incomplete ureteric bud outgrowth and failure of tubule formation in the mesenchyme. Therefore, *Sall1* is essential for ureteric bud invasion, the initial key step in metanephros development.

At present only about 20 genes are known to have important roles for kidney development and the genetic cascade of kidney development is still largely unknown. Therefore there may exist unknown mesenchymal genes that are essential for kidney development and an efficient screening assay such as microarray analysis is needed to identify these genes. We did a microarray analysis with mesenchymal cells of *Sall1-GFP* knockin mice isolated by fluorescein-activated cell sorting (FACS). In this report we show that the combination of microarray analysis and *Sall1-GFP* knockin mice, is useful for identifying many mesenchymal genes.

2. Results

2.1. Generation of Sall1-GFP knockin mice

To label *Sall1*-expressing cells, green fluorescence protein (*GFP*) was knocked in the *Sall1* locus by homologous recombination. *GFP* was inserted into the *Eco*RI site of exon 2 so that N-terminal 52 amino acids of *Sall1* were fused in frame to *GFP* (Fig. 1A). Mice were genotyped using Southern blots (data not shown). This strategy is essentially the same as those used for *Sall1*-del and *Sall1-LacZ* mice that we reported, and all homozygous mice showed kidney agenesis or severe dysgenesis (data not shown). In contrast, heterozygous mice were phenotypically normal and were used for this study.

2.2. Expression pattern of GFP fluorescence in Sall1-GFP knockin kidneys

Prominent fluorescence of *GFP* was visible through the surface of brains, kidneys and limb buds of embryonic *Sall1-GFP* heterozygous mice. Microscopic analysis of the frozen section confirmed specific expression of *GFP* in cells of mesenchymal origin. Green fluorescence was observed throughout the metanephric mesenchyme, ranging from condensed mesenchyme, S-shaped bodies, to renal tubules (Fig. 1B). This expression pattern is consistent with *LacZ* expression of *Sall1-LacZ* knockin mice generated earlier (Fig. 1C) (Nishinakamura et al., 2001). *Sall1* expression was also observed in glomeruli in *Sall1-LacZ* mice, but not in *Sall1-GFP* mice perhaps due to the low sensitivity of *GFP*. Examination of both strains revealed *Sall1* expression in stromal cells, the outer most layer of the kidney, that was not noted in our earlier study.

2.3. Isolation of GFP-expressing kidney mesenchymal cells by FACS

To isolate *GFP*-positive cells from embryonic kidneys of these *Sall1-GFP* heterozygous mice, FACS analysis was used. Embryonic kidneys (17.5 dpc) were digested with collagenase, dissociated into single cells by pipetting and sorted. *GFP*-positive cells (12% of total kidney cells) and *GFP*-negative cells (20%) were isolated (Fig. 2A), and their purity was determined by reanalysis (94% of isolated *GFP*-positive cells and 99% of isolated *GFP*-negative cells were redetected in each gate).

Gene expression of each population was examined using RT-PCR (Fig. 2B). Indeed the positive population preferentially expressed *Sall1*, *GDNF* and *WT-1*, marker genes of mesenchymal cells, while the negative population

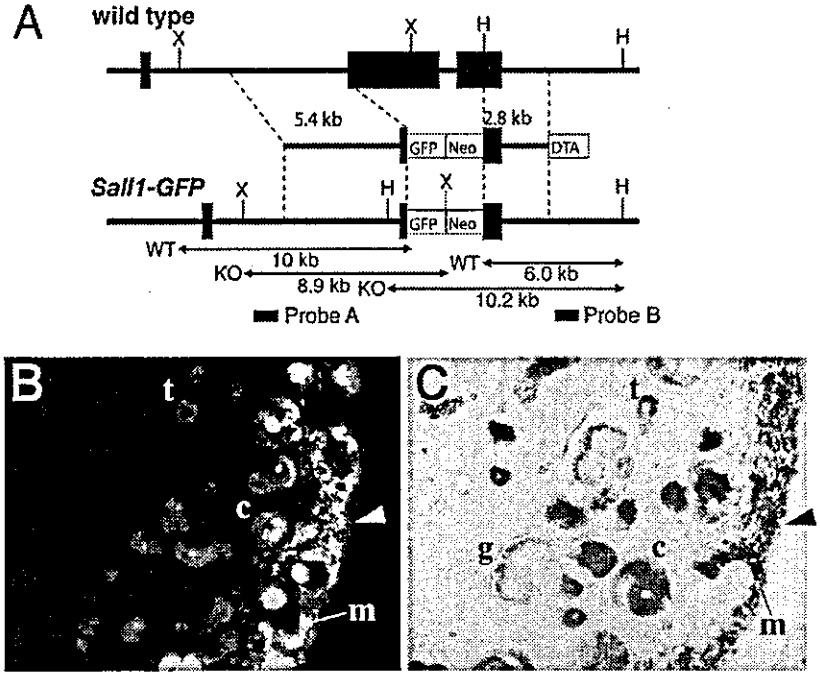

Fig. 1. Generation of *Sall1-GFP* knockin mice. (A) Targeting strategy of *Sall1-GFP* mice. *GFP* was knocked in the *Sall1* locus so that N-terminal 52 amino acids of *Sall1* was fused in frame to *GFP*. (B) *GFP* expression in embryonic kidney of heterozygous *Sall1-GFP* knockin mice. (C) X-gal staining of embryonic kidney in heterozygous *Sall1-LacZ* knockin mice. Arrowhead, stroma; m, condensed mesenchyme; c, comma-shaped bodies; t, tubles; g, glomerulus.

preferentially expressed *Ret*, a marker gene of the ureteric bud. A weak *Sall1* signal in the GFP-negative cells indicated that cells weakly expressing *Sall1* were included in the GFP-negative gate we defined in FACS analysis.

2.4. Demonstration of differential gene expression

To identify genes that are differentially expressed between *GFP*-positive and -negative populations, microarray analysis with Affymetrix GeneChip probe array was done. One microgram total RNA of each population isolated from the FACS analysis were individually amplified to 50 μg of cRNA by T7-mediated in vitro transcription, and each cRNA product was used to interrogate Mu74 GeneChips containing probe sets representing over 36,000 mouse genes and EST clusters. We identified 392 mRNAs expressed threefold greater in the *GFP*-positive population and sorted the list by the sort score determined using GeneChip software. The sort score is a ranking on the fold change and the absolute expression intensity. The higher the fold change and the absolute expression intensity become, the higher was the sort score. For example a gene whose absolute expression intensity changes from 100 in *GFP*-negative cells to 1000 in *GFP*-positive cells has a higher sort score than a gene whose absolute expression intensity changes from 1 to 10. Thus we obtained a statistical evaluation of differences in expression level of a gene based on the fold change and the absolute expression intensity.

We identified a large number of genes reported to be abundantly expressed in the metanephric mesenchyme, including *Sall1* (14-fold), *Glial cell line-derived neurotrophic factor* (*GDNF*) (39-fold), *Reelin* (14-fold), *Six-2* (9-fold), *Pax-8* (31-fold), *LRP-2* (7-fold), *PDGFc* (11-fold), *HeyL* (8-fold), *Cited-1* (8-fold), *Syndecan-4* (17-fold), *BMPR-1A* (8-fold) *WT-1* (7-fold), *FGF-10* (3-fold) and *BMP-7* (3-fold). We also detected stromal genes such as *Raldh-2* (23-fold) and *Fox D1* (6-fold), which is consistent with *Sall1* expression in this cell population. See supplementary

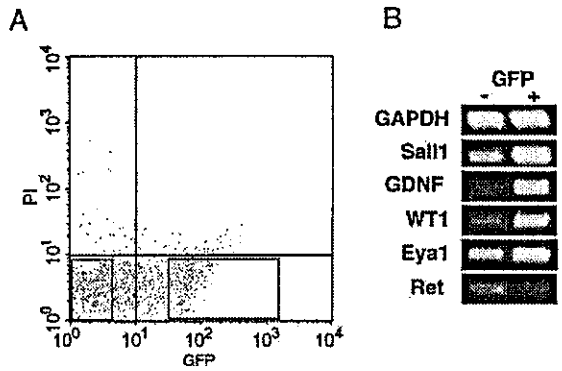

Fig. 2. FACS analysis of *Sall1-GFP* knockin embryonic kidney. (A) The distribution graph of dissociated kidney cells. We sorted *GFP*-positive (right square) and -negative population (left square). (B) RT-PCR analysis between *GFP*-positive (+) and -negative (−) population.

Table 1
Top 50 cDNAs detected abundantly in mesenchymal cells by microarray analysis

GenBank	Description	Mean (Sall1 −)	Mean (Sall1 +)	Fold change	Sort score	Test	Method
AA386439	Sall1	105.3	1531	14.2	14.68	+	Reported
D49921	GDNF	10.1	471.4	38.6	12.68	+	Reported
AJ001116	Unc4.1 homeobox	9.1	371.7	37.9	11.85	+	Reported
AW060720	Hormonally upregulated Neu-associated kinase	22.8	518	22.8	11.5	+	Reported
X99273	Raldh2	−13.7	226.1	42.5	10.16	+	Reported
AI844853	Gcnt2	−9.9	264.3	39.4	9.5	−	In situ
U24703	Reelin	42.3	577.1	14	9.12	+	Reported
AV302770	ESTs	58.1	540.3	11.8	8.69	+	In situ
AW213683	RIKEN cDNA 5730456K23 gene	10.7	445.9	18	8.06	+	In situ
D13903	Protein tyrosine phosphatase, receptor type, D	−0.9	172.3	32	7.86	+	Reported
X80338	Six2	98	880.2	9	7.79	+	Reported
AI152741	Odd-skipped related 2	−110.8	409.3	19.3	7.75	+	Reported
X57487	Paired box gene 8	0.7	161.1	31.1	7.66	+	Reported
AF030433	Dickkopf homolog 1	0	137.9	26.1	6.42	+	Reported
AI042846	LRP2	148.8	1015.3	6.9	6.38	+	Reported
AI842820	RIKEN cDNA 5730456K23 gene	49.1	485	9.9	6.29	+	In situ
M32352	Renin 2	623.6	2703.4	4.6	6.15	+	Reported
M83985	Snap91	5.4	164.5	24.4	6.06	−	In situ
AW045500	ESTs	6.7	252.5	10.2	5.82	+	In situ
AA929443	Amnionless	−35.1	223.3	13.7	5.67	−	In situ
AI851805	PDGFc	33.3	368.3	10.5	5.64	+	Reported
AV319451	Renin 1 structural	21.7	266.4	12.3	5.55	+	Reported
AI790931	Fbp1	50.2	467	8.9	5.46	+	In situ
U52842	Slc22a6	−4.1	114.5	22.2	5.4	+	In situ
X17320	Purkinje cell protein 4	1.2	111.5	22	5.36	+	Reported
AI854068	RIKEN cDNA 1110018M03 gene	81.8	567	7.4	5.33	−	In situ
AI462128	ESTs (A430091O)	90.5	649.3	7.2	5.33	+	In situ
AW208410	ESTs	36.9	377.1	9.4	5.28	−	In situ
AI314694	Nx17-pending	160.4	982.7	6	5.24	+	In situ
AI891653	ESTs	57.7	418.4	9.3	5.17	−	In situ
AI428510	RIKEN cDNA 2810004A10 gene	82.7	536	7.1	5	+	In situ
AI316329	Claudin 6	−219.9	94.7	17.8	4.75	+	In situ
AI854431	RIKEN cDNA 1110031N17 gene	135.4	793.8	5.9	4.66	−	In situ
AI604913	HeyL	44.3	365.3	8.3	4.61	+	Reported
L09192	Pyruvate decarboxylase	58.8	873	5.9	4.58	+	Reported
AI430929	Wnk4	262.3	1267.2	4.8	4.56	+	In situ
AI480529	RIKEN cDNA 6720429C22 gene	261.6	1257.4	4.8	4.51	+	In situ
X15789	Crabp1	0.4	95.6	18	4.32	+	Reported
J05663	Aldo–keto reductase family 1, member B7	64.4	321.2	7.7	4.2	+	Reported
U65091	Cited1	48.6	415.5	7.5	4.2	+	Reported
AI854068	RIKEN cDNA 1110018M03 gene	12.8	192.2	10.6	4.2	−	In situ
AA738774	Expressed sequence R75022	94.8	435.6	6.8	4.11	+	In situ
AI427519	Claudin 12	328.2	1417.6	4.3	4.09	−	In situ
AI326813	ESTs	−2.5	172.2	10.3	3.92	−	In situ
AF039391	μ-crystallin	9.8	124.4	12.7	3.87	+	In situ
AI837101	Calsyntenin 1	72.8	278.2	7.8	3.82	−	In situ
M21828	Gas2	37.8	287.8	7.6	3.77	+	In situ
D89571	Syndecan 4	−24.2	67.1	17.3	3.76	+	Reported
AA790312	ALCAM	399.9	1571.8	3.9	3.71	+	In situ
X63190	Etv4	1.8	81.3	15.2	3.56	+	In situ

Mean: expression intensity of cDNA. Test: (+) indicates that the cDNA proved to be a mesenchymal gene. (−) indicates that the cDNAs were proven to be negative. Method: Some cDNA were already noted in mesenchymal genes (Reported), and others were identified by mRNA in situ hybridization (in situ).

information for the complete data set (Supplementary information 1).

We also examined genes expressed more in *GFP*-negative cells than in the positive cells. We detected 612 mRNAs expressed threefold weaker in the *GFP*-positive cells (data not shown). We detected genes which are known to specifically expressed ureteric buds, such as *Wnt-11* (11-fold) and *TGFβ-1* (18-fold). However, many genes expressed in blood vessels were detected in these mRNAs which means that *GFP*-negative cells include not only ureteric buds but also cells derived from blood vessels.

To verify the result of microarray analysis, we subsequently did in situ hybridization for the top 50, except genes the expression patterns of which were previously

Table 2
Expression patterns of newly identified mesenchymal genes using microarray analysis

GenBank	Genes	Stromal cells	Condensed mesenchyme	S-, C-shaped bodies	Distal, proximal tubules	Glomeruli	Ureter
AI844853	Gcnt2	−	±	+	−	−	±
AV302770	ESTs	−	+	+	+	?	±
AW213683	5730456K23Rik	−	+	+	+	−	+
M83985	Snap91	−	−	±	−	−	−
AW045500	ESTs	−	+	−	−	−	−
AA929443	Amnionless	−	−	−	+	−	−
AI790931	Fbp1	−	+	+	+	+	−
U52842	Slc22a6	−	+	+	+	−	+
AI854068	1110018M03Rik	−	±	−	−	−	−
AI462128	ESTs (A430091O)	−	−	+	−	−	−
AW208410	ESTs	−	−	−	−	−	−
AI314694	Nx17-pending	−	+	+	+	?	+
AI891653	ESTs	−	−	−	−	−	−
AI428510	2810004A10Rik	−	+	+	−	−	−
AI316329	Claudin 6	−	−	−	−	−	+
AI854431	1110031N17Rik	−	−	−	−	−	−
AI430929	Wnk4	−	±	±	−	−	−
AI480529	6720429C22Rik	−	+	+	+	−	+
AA738774	R75022	−	+	+	+	−	−
AI427519	Claudin-12	−	−	−	−	−	±
AI326813	ESTs	−	−	−	−	−	−
AF039391	μ-crystallin	−	+	−	−	−	−
AI837101	Calsyntenin 1	−	−	−	−	−	−
M21828	Gas2	−	−	+	−	−	±
AA790312	ALCAM	+	−	−	−	−	−
X63190	Etv4	−	+	+	+	−	+
AI838599	ESTs	−	−	−	−	−	−
AI837711	ESTs(AK049098)	+	−	−	−	−	−
AI843433	ESTs(AW049604)	−	−	−	−	−	−
AI851210	ESTs(AK081204)	−	−	−	−	−	−
AI315647	Cors26	−	−	−	−	−	−
AW120700	ESTs(AW120700)	−	+	±	±	+	±
AI891500	1700011H14Rik	−	−	−	−	−	+
AI503543	SSB-4	−	±	+	−	−	+
AI838112	Smarcd3	−	+	−	−	−	+
AI152966	FLJ22569	−	+	−	−	−	±
AA727914	ESTs(AV158822)	−	−	−	−	−	+
AI836553	1110038H03Rik	−	±	+	−	−	−
AV071536	ESTs	−	−	−	−	−	±
AI463306	AW555464	−	+	+	−	−	−
AU021802	ESTs	−	−	−	−	−	−
AV336991	ESTs	−	−	−	−	−	−
AW124490	3000002J10Rik	−	±	−	−	−	−
AW050290	2810406K24Rik	−	+	−	−	−	−
AI842510	TRB-2	−	−	−	−	+	−

The expression pattern of each cDNAs was classified based on compartments of the kidney. The cDNAs were listed in order of sort score. The expression levels are represented by: (+) abundantly, (−) not detected, (±) weakly, (?) unknown.

reported (Table 1). The expression patterns of most of the genes were in good correlation with the results of our microarray analysis. 78% of the top 50 was confirmed to be expressed in the condensed mesenchyme, stromal cells, metanephric tubles or glomeruli. Out of top 50 mRNAs, 22 were previously reported as mesenchymal genes, 17 are newly identified ones as mesenchymal genes in the present work and 11 are not expressed in the mesenchyme. This indicates that most of the genes detected in the *GFP*-positive population using microarray analysis are indeed expressed abundantly in cells of mesenchymal origin or stromal cells.

2.5. Expression pattern of novel mesenchymal genes in the developing kidney

To determine which cells of the developing kidney express mesenchymal genes detected by microarray analysis, in situ hybridization with selected mRNAs was

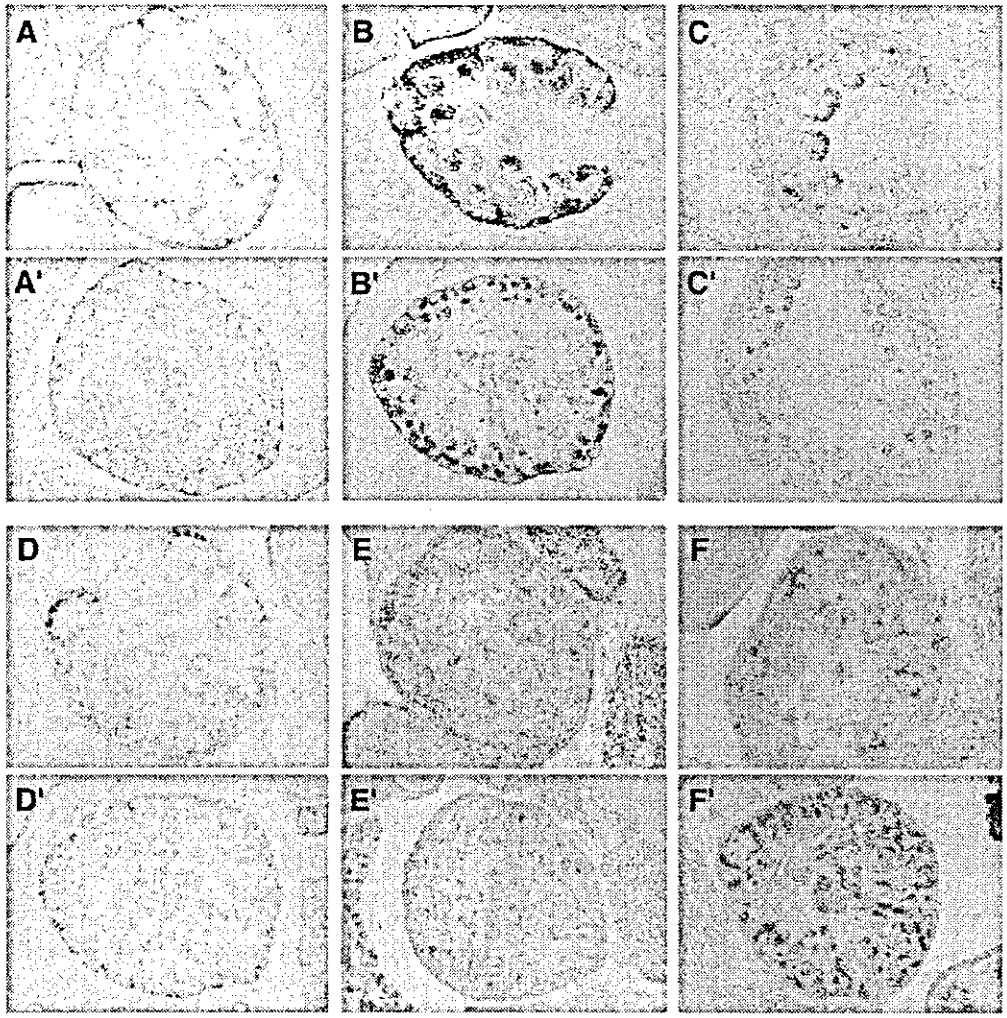

Fig. 3. In situ hybridization of fetal kidney. Upper panels are sections of 14.5 dpc and lower panels are those of 17.5 dpc. (A), (A′) *ALCAM*. (B), (B′) *Raldh2*. (C), (C′) *TRB-2*. (D), (D′) *μ-crystallin*. (E), (E′) *Smarcd3*. (F), (F′) *SSB-4*.

done (Table 2). We examined the top 50 mRNAs as well as mRNAs which gave high 'fold change' or high 'absolute expression intensity' in GFP-positive cells. We found that many genes defined as mesenchymal by microarray analysis were indeed expressed in the metanephric mesenchyme, including *ALCAM, SSB-4, Smarcd3, μ-crystallin, TRB-2*. These genes have not been previously reported as mesenchymal genes. In situ hybridization of these genes at two stages is shown in Fig. 3 (Supplementary information 2 for detailed images). 14.5 dpc is the stage representing development of the nephron in process, and 17.5 dpc is the stage at which RNA samples were collected.

ALCAM was first identified on thymic epithelial cells (Patel et al., 1995). *ALCAM* is a member of the Ig superfamily containing five extracellular Ig domains, and it activates leukocytes (Bowen et al., 1995). Arai et al. reported that *ALCAM*-positive perichondrial cells can differentiate into multiple lineages and the addition of *ALCAM*-Fc to metatarsal cultures inhibits the invasion of the blood vessels to a cartilage (Arai et al., 2002). We found that *ALCAM* was expressed abundantly in stromal cells, consisting with *Sall1* expression in the stromal region (Fig. 3A,A′).

The *Raldh2* gene codes for a retinaldehyde dehydrogenase that catalyzes the second oxidative step in the biosynthesis of retinoic acid (RA) from retinol (Zhao et al., 1996). *Raldh2* is responsible for most of the RA-synthesizing activity during early mouse embryogenesis (7.5–9.5 dpc), as seen from the failure of *Raldh2* −/− embryos to activate RA-responsive transgenes (Niederreither et al., 1999). These mutant embryos, which die at E9.5–10.5 from severe cardiac defects, exhibit axial truncation due to impaired somite growth, as well as hindbrain defects

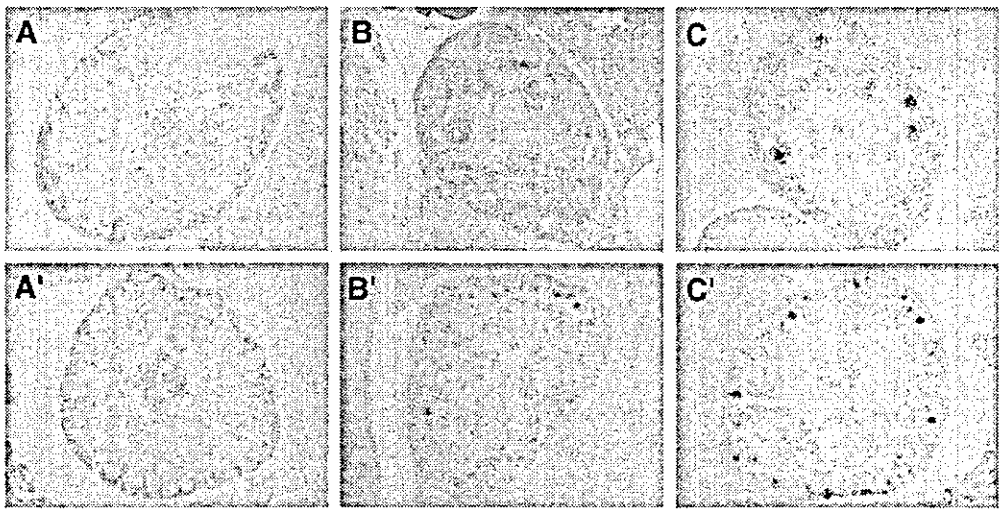

Fig. 4. In situ hybridization of ESTs in the fetal kidney. Upper panels are sections of 14.5 dpc and lower panels are those of 17.5 dpc. (A), (A′) BC023483. (B), (B′) 2810004A10Rik. (C), (C′) 1110038H03Rik.

(Niederreither et al., 1999, 2000, 2001). Our in situ hybridization showed *Raldh2* to be expressed in the stromal region (Fig. 3B,B′). Identification of two stromal genes (*ALCAM* and *Raldh2*) further proves that *Sall1* is also expressed in the stromal region.

TRB-2 is a mammalian homolog of *Drosophila tribbles*, which causes the degradation of *String/CDC25* and blocks mitosis. *TRB-2* was specifically expressed in the comma-, S-shaped bodies and glomeruli (Fig. 3C,C′). *TRB-3* was shown to be involved in insulin signaling (Du et al., 2003), which was the first demonstration that this family is important in mammals.

μ-crystallin is one of the taxon-specific crystallins and the predicted amino acid sequence indicates that *μ-crystallin* might have an enzymatic rather than a structural role in lens tissue (Kim et al., 1992; Vie et al., 1997). We specifically detected *μ-crystallin* in the condensed mesenchyme of the metanephric kidney (Fig. 3D,D′).

Smarcd3 is the member of the SWI/SNF family, the members of which display helicase and ATPase activities and which are thought to regulate transcription of certain genes by altering the chromatin structure around those genes (Ring et al., 1998). The encoded protein is part of the large ATP-dependent chromatin remodeling complex SNF/SWI. Our in situ hybridization showed *Smarcd3* to be abundantly expressed in the condensed mesenchyme, S-, comma-shaped bodies and weakly in the ureteric buds and collecting ducts (Fig. 3E,E′).

SSB-4 is a member of family of proteins that contain a C-terminal SOCS box and a SPRY domain. *SSB-4* was expressed abundantly in the condensed mesenchyme, glomerulus and weakly in ureteric buds and collecting ducts (Fig. 3F,F′).

We also examined expression patterns of some ESTs (Fig. 4). BC023483 was specifically expressed in the condensed mesenchyme (Fig. 4A). 2810004A10Rik was expressed abundantly in the S-, comma-shaped bodies and weakly in the condensed mesenchyme (Fig. 4B). 1110038H03Rik was expressed abundantly in S-, comma-shaped bodies and weakly in the condensed mesenchyme (Fig. 4C).

Taken together, it is evident that a combination of microarray analysis and *Sall1-GFP* knockin mice is useful for identification of kidney mesenchymal genes.

2.6. Mesenchymal genes in Sall1 knockout mice

This analysis also means that detected genes should colocalize with *Sall1* at various stages of metanephric development. The genes detected using our microarray analysis possibly include genes interacting with *Sall1*, genes downstream or upstream of *Sall1*, and these candidate genes could be essential for metanephric development. Colocalization of candidate genes with *Sall1* allows one to hypothesize that those genes could be regulated by critical transcription factors for kidney development, including *Sall1*. To clarify whether detected genes are downstream targets of *Sall1*, in situ hybridization in the developing kidney of *Sall1* knockout mice was done (11.5 dpc). At 11.5 dpc, uninduced condensed mesenchyme exists in *Sall1* knockout mice, but is reduced in size. We found 10 genes in the top 50 that were expressed in the condensed mesenchyme at 11.5 dpc. In *Sall1* knockout mice, expression levels of all the genes were either intact (*Six2, Raldh2, PDGFc, ALCAM, Hunk, Gas2, μ-crystallin*) or reduced (*Pax8, Unc4.1, GDNF*) (Fig. 5 and data not shown), and no gene was completely absent. Reduction in expression level of some genes could occur by metanephric mesenchymal reduction in size in *Sall1* knockout mice (Nishinakamura et al., 2001). In this case, transcription

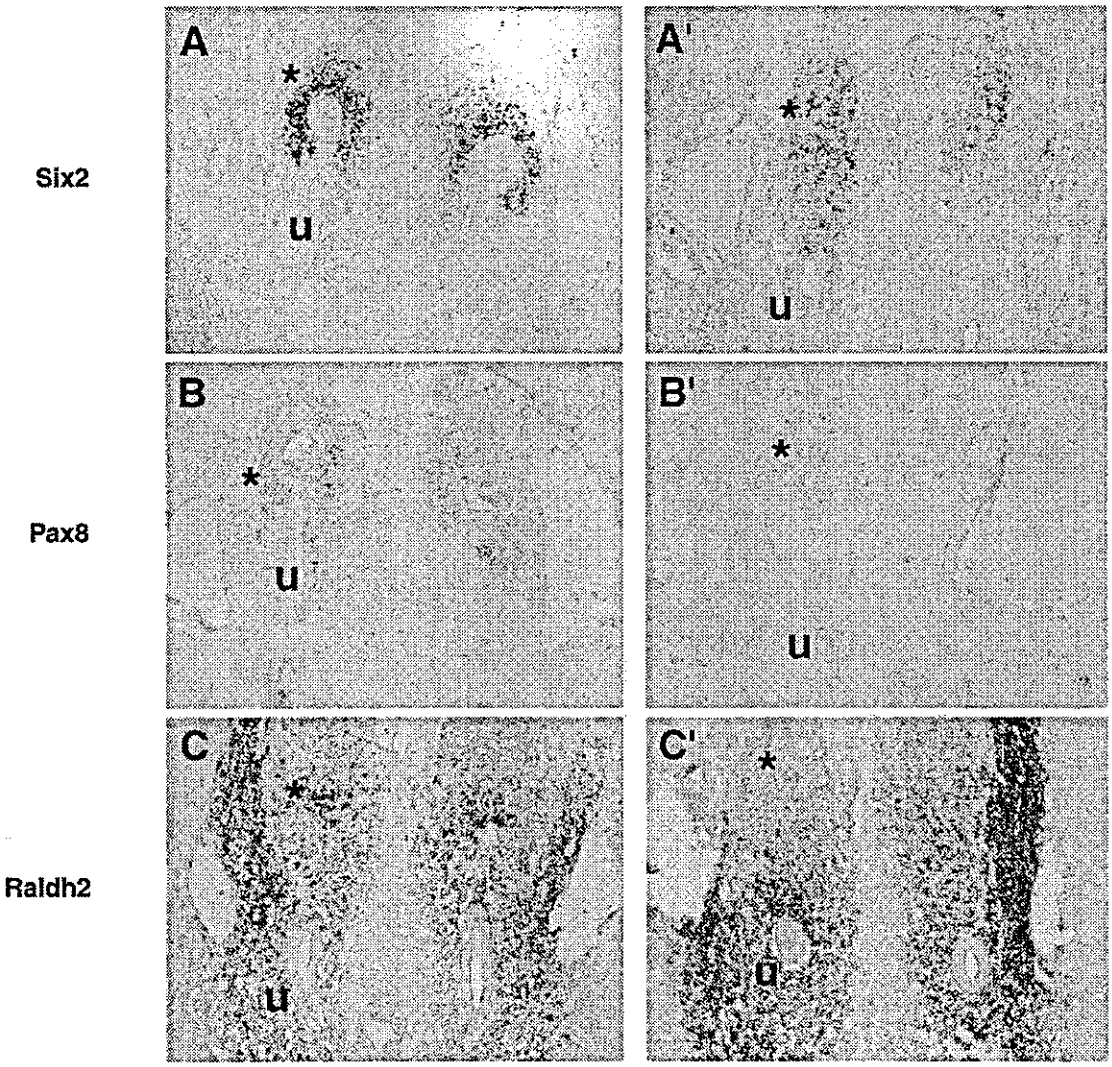

Fig. 5. In situ hybridization of mesenchymal genes in *Sall1* knockout (A′,B′,C′) and wild type mice (A,B,C) at 11.5 dpc. (A), (A′) *Six2*. (B), (B′) *Pax8*. (C), (C′) *Raldh2*. u, ureteric buds; asterisk (*), condensed mesenchyme.

factors other than *Sall1* could regulate the candidate genes, and utilization of mice lacking other critical transcription factors would be needed to clarify genetic cascades involved in candidate genes detected in this present work. Alternatively it could be possible that they are downstream targets of *Sall1* and loss of *Sall1* is compensated for by other transcription factors or *Sall* family genes (*Sall2, Sall3* and *Sall4*). To demonstrate this possibility, generating mice lacking both *Sall1* and another transcription factor or mice lacking all the *Sall* family genes is awaited.

3. Discussion

In the developing kidney, *Sall1* is expressed in the stroma region and cells of mesenchymal origin, including condensed mesenchyme, S-, comma-shaped bodies, podocytes, Bowman's capsule and distal, proximal tubles, while cells not expressing *Sall1* are collecting ducts, ureteric buds, medullary zone and blood vessels. This means that a comparison analysis of gene expression profiles in *Sall1*-positive and -negative cells can identify mesenchymal genes. Indeed we could detect many well-known mesenchymal genes using microarray analysis, including *GDNF, Raldh-2, Reelin, Six-2, Pax-8, LRP-2, PDGFc, HeyL, Cited-1, Syndecan-4, BMPR-1A, WT-1, FoxD1, FGF-10* and *BMP-7*. Our in situ hybridization analysis showed that 78% of the top 50 mRNAs of the microarray list were specifically expressed in cells of mesenchymal origin or the stroma. This supports the notion that many mesenchymal genes are enriched in *Sall1*-positive cells. Moreover we found unknown mesenchymal genes and ESTs that are expressed

in cells of mesenchymal origin, using in situ hybridization, including *μ-crystallin, ALCAM, SSB-4, Smarcd3* and *TRB-2*. Thus we demonstrate that a combination of microarray technology and *Sall1-GFP* knockin mice is useful for efficient identification of mesenchymal genes expressed in the developing kidney.

Though kidney development is indeed a complicated system, no more than 20 genes have been identified as being essential. In this report, we identified a large number of mesenchymal genes in the developing kidney. To find essential genes from this large list, efficient and rapid screening is needed. Recently emerging siRNA technology is one potent method. Indeed Sakai et al. reported that transfection of siRNA into the metanephros followed by organ culture was useful for demonstrating essential roles of fibronectin in the developing kidney (Sakai et al., 2003). A similar approach could be used for our candidate genes. However, interpretation can be risky. A variety of genes was reported to be essential for kidney development, using conventional antisense oligo nucleotides and organ culture technology, but many proved negative when subjected to gene targeting. Therefore generating knockout mice of each candidate gene is necessary for proof. Establishment of a kidney-specific knockout system could also be useful for the purpose.

We showed that *Sall1, GDNF*, and *Raldh-2*, the genes essential for metanephric development, rank high in our gene chip list. *GDNF* is expressed in the metanephric mesenchyme before ureteric bud initiation. Null mutation of *GDNF* has severe kidney phenotypes, ranging from no ureteric bud formation to rudimentary kidney formation, which is very close to the phenotype of *Sall1* mutant mice. Retinaldehyde dehydrogenase-2 (*Raldh2*) is required for most embryonic RA synthesis (Niederreither et al., 1999) and is expressed in stromal cells (Fig. 3F,F′). *Raldh2, RARα* and *RARβ2* are colocalized in the cortical stroma, and knockout mouse studies showed that RA is important in the cortical stroma for generating signals that control branching morphogenesis by regulating *Ret* expression in the ureteric bud (Batourina et al., 2001). *Sall1* could be involved in these *GDNF-Ret* and/or RA-*Ret* pathways, though *Raldh2* is unlikely to be a downstream target of *Sall1*, as shown by intact *Raldh2* expression in *Sall1* knockout mice (Fig. 5C).

In conclusion, we identified many mesenchymal genes, and demonstrated that using a combination of microarray technology and *Sall1-GFP* knockin mouse is a pertinent means of identifying mesenchymal genes systematically. A similar approach may be applicable to other organs, such as brains and limb buds where *Sall1* is expressed.

4. Experimental procedures

4.1. Generation of GFP knockin mice

A Sal-NotI *GFP* fragment (769 bp) from pEGFP-N1 (Clontech) was fused to the *Sal*I-*Pac*I site of pxCAN-LacZ (RIKEN), then the 5′ *Sma*I-*Sma*I 5.4 kb fragment was fused to the *Bam*HI site of this vector in frame. Finally, the resultant *Sal*I-*Xho*I 6.7 kb fragment was cloned into the *Xho*I site of the vector, that contained the neomycin-resistant (neo^r) gene (pMC1-neo polyA), 3′ *Hin*dIII-*Cla*I 2.8 kb fragment and a diphtheria toxin A subunit (pMC1-DTA) in tandem.

E14.1 embryonic stem cells were plated on mitomycin C-treated primary embryonic fibroblasts, and clones resistant to G418 (400 μg/ml) were screened using Southern blots. The genomic DNA from clones was digested with *Hin*dIII, electrophoresed through 0.7% agarose, transferred to nylon membrane (HybondN +, Amersham-Pharmacia), and hybridized to a radioactive probe. The probe used to screen the samples was a *Cla*I-*Eco*RI 1.2 kb fragment downstream of 3′ homology (probe B). The samples were also digested with *Xho*I, and hybridized with a 5′ probe (probe A) to confirm the correct homologous recombination. A probe corresponding to the Neo sequence was also used to verify that only one copy of the vector was integrated into the genome. Of 120 clones, six were correctly targeted for *Sall1-GFP*.

Recipient blastocysts were from C57BL/6J mice. Chimeric animals were bred with C57BL/6J females. Mutant animals studied were of F_2 and F_3 generations. Mice were genotyped using Southern blots or genomic PCR. The primer sequences used for PCR were as follows: AGCTAAAGCTGCCAGAGTGC, CAACTTGCGATT GCCAT AAA, and GCGTTGGCTACCCGTGATAT (288 bp for the wild-type Sall1 allele, and 350 bp for the mutated allele).

4.2. Fluorescein-activated cell sorting

Cell suspension was prepared from kidney of *Sall1-GFP* knockin mice (17.5 dpc). Kidneys were digested with 0.25% collagenase type B (Roche Diagnostics) at 37 °C for 1 h, and cells were dissociated using fine-tipped pipettes. After the cells had been filtered through a 35 μm nylon mesh, they were resuspended in PBS containing 0.5% FCS and 1 mM EDTA at a final concentration of 2×10^6 cells/ml. Propidium Iodide (Sigma-Aldrich) was added at a final concentration of 50 μg/ml to label the dead cells.

FACS analysis was done with the FACS Vantage (Becton Dickinson Immunocytometry Systems). Dead cells were excluded from the plots based on propidium iodide. The isolated cells were centrifuged at 1000 rpm for 5 min and resuspended in TRIzol Reagent (Invitrogen).

4.3. RNA amplification for array analysis

MessageAmp™ aRNA Kits (Ambion) were used according to the manufacturer's instructions. Briefly, 11 μl of 1 μg total RNA and 1 μl of T7-Oligo(dT) Primer incubated at 70 °C for 10 min, was followed by incubation at 42 °C for 5 min. Next, 2 μl of 10× First Strand Buffer, 1 μl of Ribonuclease Inhibitor and 4 μl of dNTP Mix were added,

and incubation continued at 42 °C for 2 h. Next, 63 μl of RNase-free H_2O, 10 μl of 10 × Second Strand Buffer, 4 μl of dNTP Mix, 2 μl of DNA Polymerase and 1 μl of RNase H, and the mixture was incubated at 16 °C for 2 h. Next, the cDNA was purified, and dried down to 8 μl for in vitro transcription. For in vitro transcription, 8 μl of the purified cDNA, dried biotin-CTP and -UTP, 2 μl of T7 ATP Solution (75 mM), 1.5 μl of T7 CTP Solution (75 mM), 2 μl of T7 GTP Solution (75 mM), 1.5 μl of T7 UTP Solution (75 mM), 2 μl of Enzyme Mix, and 1 μl of RNase-free H_2O were incubated at 37 °C for 12 h. Then 2 μl of DNase 1 was added and incubated at 37 °C for 30 min, followed by antisense RNA purification.

4.4. Microarray analysis

The Affymetrix Murine Genome U74v2 Set was used to compare gene expression profiles of the GFP-positive and -negative cells according to manufacturer's protocols. Briefly, biotinylated cRNAs were synthesized and hybridized to the GeneChip probe arrays, which were then washed in washing solution, stained with streptavidin–phycoerythrin and scanned. Analysis was made using Affymetrix GeneChip software. Two independent RNA samples were prepared and similar results were obtained using Mu74A GeneChip, then one of two samples was used for Mu74 complete GeneChip (Mu74A, B and C).

4.5. In situ hybridization

In situ hybridization was done using digoxigenin-labeled antisense riboprobes as described (Nishinakamura et al., 2001). Fragments were amplified using PCR, subcloned into pCRII (Invitrogen), and sequenced. None of the sense probes yielded signals.

Acknowledgements

We thank Miyuki Itoh for technical assistance. The Division of Stem Cell Regulation is supported by Amgen Limited. The work was partly supported by grants from Research for the Future Program in Ministry of Education, Science, Technology, Sports and Culture, Japan.

References

Arai, F., Ohneda, O., Miyamoto, T., Zhang, X.Q., Suda, T., 2002. Mesenchymal stem cells in perichondrium express activated leukocyte cell adhesion molecule and participate in bone marrow formation. J. Exp. Med. 195, 1549–1563.

Batourina, E., Gim, S., Bello, N., Shy, M., Clagett-Dame, M., Srinivas, S., et al., 2001. Vitamin A controls epithelial/mesenchymal interactions through Ret expression. Nat. Genet. 27, 74–78.

Bowen, M.A., Patel, D.D., Li, X., Modrell, B., Malacko, A.R., Wang, W.C., et al., 1995. Cloning, mapping, and characterization of activated leukocyte-cell adhesion molecule (ALCAM), a CD6 ligand. J. Exp. Med. 181, 2213–2220.

Buller, C., Xu, X., Marquis, V., Schwanke, R., Xu, P.X., 2001. Molecular effects of Eya1 domain mutations causing organ defects in BOR syndrome. Hum. Mol. Genet. 10, 2775–2781.

Cacalano, G., Farinas, I., Wang, L.C., Hagler, K., Forgie, A., Moore, M., et al., 1998. GFRalpha1 is an essential receptor component for GDNF in the developing nervous system and kidney. Neuron 21, 53–62.

Du, K., Herzig, S., Kulkarni, R.N., Montminy, M., 2003. TRB3: a tribbles homolog that inhibits Akt/PKB activation by insulin in liver. Science 300, 1574–1577.

Herzlinger, D., Koseki, C., Mikawa, T., al-Awqati, Q., 1992. Metanephric mesenchyme contains multipotent stem cells whose fate is restricted after induction. Development 114, 565–572.

Kim, R.Y., Gasser, R., Wistow, G.J., 1992. mu-crystallin is a mammalian homologue of Agrobacterium ornithine cyclodeaminase and is expressed in human retina. Proc. Natl Acad. Sci. USA 89, 9292–9296.

Kohlhase, J., Schuh, R., Dowe, G., Kuhnlein, R.P., Jackle, H., Schroeder, B., et al., 1996. Isolation, characterization, and organ-specific expression of two novel human zinc finger genes related to the Drosophila gene spalt. Genomics 38, 291–298.

Kohlhase, J., Wischermann, A., Reichenbach, H., Froster, U., Engel, W., 1998. Mutations in the SALL1 putative transcription factor gene cause Townes-Brocks syndrome. Nat. Genet. 18, 81–83.

Kohlhase, J., Hausmann, S., Stojmenovic, G., Dixkens, C., Bink, K., Schulz-Schaeffer, W., et al., 1999. SALL3, a new member of the human spalt-like gene family, maps to 18q23. Genomics 62, 216–222.

Kohlhase, J., Altmann, M., Archangelo, L., Dixkens, C., Engel, W., 2000. Genomic cloning, chromosomal mapping, and expression analysis of msal-2. Mamm. Genome 11, 64–68.

Kohlhase, J., Heinrich, M., Schubert, L., Liebers, M., Kispert, A., Laccone, F., et al., 2002. Okihiro syndrome is caused by SALL4 mutations. Hum. Mol. Genet. 11, 2979–2987.

Kreidberg, J.A., Sariola, H., Loring, J.M., Maeda, M., Pelletier, J., Housman, D., et al., 1993. WT-1 is required for early kidney development. Cell 74, 679–691.

Kuhnlein, R.P., Frommer, G., Friedrich, M., Gonzalez-Gaitan, M., Weber, A., Wagner-Bernholz, J.F., et al., 1994. Spalt encodes an evolutionarily conserved zinc finger protein of novel structure which provides homeotic gene function in the head and tail region of the Drosophila embryo. Eur. Mol. Biol. Org. J. 13, 168–179.

Moore, M.W., Klein, R.D., Farinas, I., Sauer, H., Armanini, M., Phillips, H., et al., 1996. Renal and neuronal abnormalities in mice lacking GDNF. Nature 382, 76–79.

Niederreither, K., Subbarayan, V., Dolle, P., Chambon, P., 1999. Embryonic retinoic acid synthesis is essential for early mouse post-implantation development. Nat. Genet. 21, 444–448.

Niederreither, K., Vermot, J., Schuhbaur, B., Chambon, P., Dolle, P., 2000. Retinoic acid synthesis and hindbrain patterning in the mouse embryo. Development 127, 75–85.

Niederreither, K., Vermot, J., Messaddeq, N., Schuhbaur, B., Chambon, P., Dolle, P., 2001. Embryonic retinoic acid synthesis is essential for heart morphogenesis in the mouse. Development 128, 1019–1031.

Nishinakamura, R., Matsumoto, Y., Nakao, K., Nakamura, K., Sato, A., Copeland, N.G., et al., 2001. Murine homolog of SALL1 is essential for ureteric bud invasion in kidney development. Development 128, 3105–3115.

Patel, D.D., Wee, S.F., Whichard, L.P., Bowen, M.A., Pesando, J.M., Aruffo, A., et al., 1995. Identification and characterization of a 100-kD ligand for CD6 on human thymic epithelial cells. J. Exp. Med. 181, 1563–1568.

Pichel, J.G., Shen, L., Sheng, H.Z., Granholm, A.C., Drago, J., Grinberg, A., et al., 1996. Defects in enteric innervation and kidney development in mice lacking GDNF. Nature 382, 73–76.

Ring, H.Z., Vameghi-Meyers, V., Wang, W., Crabtree, G.R., Francke, U., 1998. Five SWI/SNF-related, matrix-associated, actin-dependent

regulator of chromatin (SMARC) genes are dispersed in the human genome. Genomics 51, 140–143.

Sainio, K., Suvanto, P., Davies, J., Wartiovaara, J., Wartiovaara, K., Saarma, M., et al., 1997. Glial-cell-line-derived neurotrophic factor is required for bud initiation from ureteric epithelium. Development 124, 4077–4087.

Sakai, T., Larsen, M., Yamada, K.M., 2003. Fibronectin requirement in branching morphogenesis. Nature 423, 876–881.

Sanchez, M.P., Silos-Santiago, I., Frisen, J., He, B., Lira, S.A., Barbacid, M., 1996. Renal agenesis and the absence of enteric neurons in mice lacking GDNF. Nature 382, 70–73.

Schuchardt, A., D'Agati, V., Larsson-Blomberg, L., Costantini, F., Pachnis, V., 1994. Defects in the kidney and enteric nervous system of mice lacking the tyrosine kinase receptor Ret. Nature 367, 380–383.

Vie, M.P., Evrard, C., Osty, J., Breton-Gilet, A., Blanchet, P., Pomerance, M., et al., 1997. Purification, molecular cloning, and functional expression of the human nicodinamide-adenine dinucleotide phosphate-regulated thyroid hormone-binding protein. Mol. Endocrinol. 11, 1728–1736.

Xu, P.X., Adams, J., Peters, H., Brown, M.C., Heaney, S., Maas, R., 1999. Eya1-deficient mice lack ears and kidneys and show abnormal apoptosis of organ primordia. Nat. Genet. 23, 113–117.

Xu, P.X., Zheng, W., Huang, L., Maire, P., Laclef, C., Silvius, D., 2003. Six1 is required for the early organogenesis of mammalian kidney. Development 130, 3085–3094.

Zhao, D., McCaffery, P., Ivins, K.J., Neve, R.L., Hogan, P., Chin, W.W., et al., 1996. Molecular identification of a major retinoic-acid-synthesizing enzyme, a retinaldehyde-specific dehydrogenase. Eur. J. Biochem. 240, 15–22.

J Am Soc Nephrol 15: 3083–3092, 2004

Expression and Function of Ets-1 during Experimental Acute Renal Failure in Rats

HIROYUKI TANAKA,* YOSHIO TERADA,* TAKAHIKO KOBAYASHI,* TOMOKAZU OKADO,* SEIJI INOSHITA,* MICHIO KUWAHARA,* ARUN SETH,† YASUFUMI SATO,‡ and SEI SASAKI*

**Homeostasis Medicine and Nephrology, Tokyo Medical and Dental University, Tokyo, Japan; †Department of Laboratory Medicine and Pathology, MRC Group in Periodontal Physiology, University of Toronto, Toronto, Ontario, Canada; and ‡Department of Vascular Biology, Institutes of Development, Aging and Cancer, Tohoku University, Sendai, Japan*

Abstract. The Ets family of transcription factors is defined by a conserved DNA-binding Ets domain that forms a winged helix-turn-helix structure motif. The Ets family is involved in a diverse array of biologic functions, including cellular growth, migration, and differentiation. The hypothesis in this study was that Ets-1 is re-expressed during regeneration after acute renal failure (ARF) and plays a key role in the transcriptional regulation of cyclin D1 and the cell cycle progression in renal tubular cells. For clarifying the significance of Ets-1 in ARF, a rat ARF model *in vivo* and LLC-PK1 cells as an *in vitro* model were used. After the left rat renal artery was clamped for 1 h, the whole kidney homogenate was examined and total RNA was extracted at 6, 12, 24, 48, and 72 h after reperfusion by Western blot analysis and real-time reverse transcription–PCR. Ets-1 mRNA and protein expression were strongly increased at 6 to 24 h after the ischemia, respectively. The expression of hypoxia-inducible factor-1α was increased dramatically as early as 6 h after ischemia-reperfusion and decreased at 48 and 72 h after ischemia-reperfusion. In the immunohistologic examination, Ets-1 was expressed in the proximal tubules and coexpressed with proliferating cell nuclear antigen (PCNA). Furthermore, overexpression of Ets-1 promoted the cell cycle and increased the promoter activity and protein expression of cyclin D1 in LLC-PK1 cells. Ets-1 promoter activity increased between 3 and 6 h in hypoxia, and hypoxia also induced changes in the Ets-1 protein level in LLC-PK1 cells. The Ets-1 induction by hypoxia was abolished by the transfection of dominant-negative hypoxia-inducible factor-1α. A gel shift assay demonstrated that Ets-1 binds to the ets-1 binding site of the cyclin D1 promoter in the ischemia-reperfusion condition. Overexpression of Ets-1 did not significantly change the caspase 3 activity or the value of cell death ELISA in LLC-PK1 cells. Taken together, these data suggest that Ets-1 plays a key role in the cell-cycle progression of renal tubules in ARF. The Ets-1 pathway may regulate the transcription of cyclin D1 and control the regeneration of renal tubules in ARF.

Ischemic acute renal failure (ARF) is the most common form of ARF in the adult population. The molecular basis of the events that lead to tubular regeneration after ARF is not understood (1–3). An understanding of the mechanisms that lead to renal cell proliferation and regeneration will be necessary for the exploration of novel therapeutic strategies for the treatment of ischemic ARF. It has been suggested that regeneration processes may recapitulate developmental processes to restore organ or tissue function (4,5). Adult tubular epithelial cells have a potent ability to regenerate after cellular damage. After ischemic renal damage, normally quiescent cells undergo dedifferentiation and acquire the ability to proliferate after their DNA synthesis is enhanced (6,7). In ARF, the regulation of cyclin and the cyclin-dependent kinase (CDK) inhibitor have been reported (8,9). The restriction point of the G1-to-S phase is determined by the activities of cyclin D1, cyclin A, cyclin E, and CDK (10,11). Cyclin D1 and cyclin A play key roles in the G1-S regulation of renal tubular epithelial cells (12).

The Ets family of transcription factors is defined by a conserved DNA-binding Ets domain that forms a winged helix-turn-helix structure motif (13,14). This family of transcription factors is involved in a diverse array of biologic functions, including cellular growth, migration, and differentiation (14–16). Ets-1 is the first member discovered in the Ets family of transcription factors. The expression of Ets-1 has been detected in various cells, and the roles of the Ets-1 gene expressed in mesodermal lineage cells, such as fibroblasts and endothelial cells, has drawn wide attention in the fields of embryogenesis and angiogenesis (17–20). During morphogenesis, Ets-1 expression occurs in vascular structures and branching tissues, including kidneys (18,21,22). In adult tissues, the levels of Ets-1 expression are much lower than in embryonic tissues, including the kidneys (18). Ets-1 expression has been reported in mesangial cells and to increase in the glomeruli and inter-

Received September 1, 2003. Accepted September 2, 2004.
Correspondence to Dr. Yoshio Terada, Homeostasis Medicine and Nephrology, Tokyo Medical and Dental University, 5-45, Yushima 1-chome, Bunkyo-ku, Tokyo 113-8519, Japan. Phone: 81-3-5803-5214; Fax: 81-3-5803-5215; E-mail: yterada.kid@tmd.ac.jp

1046-6673/1512-3083
Journal of the American Society of Nephrology

DOI: 10.1097/01.ASN.0000145459.54236.D3

stitium in rat crescentic glomerulonephritis (23,24). However, there have been no reports concerning Ets-1 expression during ARF. Recently, we and another group reported that the developmental genes Wnt-4 and Pax2 are expressed during ischemic acute renal injury and that Wnt-4 expression promotes the proliferation of renal tubular cells (25,26). These data suggested that some developmental genes are re-expressed during the recovery phase of ARF. A recent paper demonstrated that hypoxia induced Ets-1 expression *via* the activity of hypoxia-inducible factor-1 (HIF-1) in endothelial cells (27). Thus, there is a possibility that Ets-1, which is expressed during renal development, may play roles in ischemic renal failure.

Our hypothesis in this study is that Ets-1 is re-expressed during regeneration after ARF and plays a key role in the transcriptional regulation of cyclin D1 and in the cell-cycle progression in renal tubular cells. To test this hypothesis, we examined the expression pattern of Ets-1 during the recovery phase of an ischemia-reperfusion kidney. Our data demonstrate that Ets-1 is upregulated in the early phase of an ischemia-reperfusion kidney and that the overexpression of Ets-1, using an adenovirus, regulates the transcription of cyclin D1 and cell-cycle progression in renal tubular cells.

Materials and Methods

Cell Culture and Exposure to Hypoxia

LLC-PK1 cells, originally purchased from American Type Culture Collection (Rockville, MD), were grown in DMEM (Life Technologies, Gaithersburg, MD) supplemented with 50 IU/ml penicillin, 50 μg/ml streptomycin, and 10% heat-inactivated FCS (Life Technologies). Cells were cultured at 37°C in 20% O_2 and 5% CO_2 (referred to as the normoxic condition). For the hypoxia experiments, cells were placed in a hypoxic chamber (Bellow Glass, Vineland, NJ) that contained 0% O_2 and 5% CO_2, which was maintained at 37°C.

Plasmid Constructs

The Ets-1 reporter construct used for the luciferase assays contained a mouse Ets-1 promoter (−2.1 kbp) cloned upstream of the luciferase gene (28). The cyclin D1 reporter construct used for the luciferase assays contained a human cyclin D1 promoter from residues −944 to 139 cloned upstream of the luciferase gene (a gift of Dr. M. Eilers Zentrum für Molekularbiologie Heidelberg, Heidelberg, Germany) (29). Expression vectors coding for HIF-1α and dominant-negative (dn) HIF-1α were prepared as described previously (30,31) using the following primers: forward 5'-GGAAGACAACGCGGGCAC-3' and reverse 5'-GGAGCTGTGAATGTGCTGTGATCTGGC-3' and dnHIF-1α forward 5'-CCGCTCGAGACCATGCGAAGCAAAGAGTCTG-3' and reverse 5'-GGGGTACCTCACTTATCAAAAAGGCAGCT-3'. An open reading frame coding for the dnHIF-1α is a 1.1-kbp fragment whose product lacks both the DNA binding and transactivation domain. In both cases, RNA out of a C57BL mouse kidney was used as a template. The PCR fragment was subcloned into pcDNA3.1 (Invitrogen, San Diego, CA) and was processed to dideoxy-DNA sequencing.

Transient Transfection and Luciferase Assay

LLC-PK1 cells were transfected by the electroporation method with plasmid DNA (10 μg). Data are representative of at least four independent experiments performed in duplicate and are expressed as an n-fold increase in the luciferase activity calculated relative to the indicated level of Ets-1 promoter activity. Normalization was achieved by co-transfecting a β-galactosidase reporter construct, as described previously (12). Luciferase and β-galactosidase activities were measured according to the Promega (Madison, WI) protocol.

Recombinant Adenoviruses

Replication-defective, recombinant adenoviruses encoding human Ets-1 (Adets-1) and a control adenovirus (Adnull) were prepared as described previously (32). Replication-defective, recombinant adenoviruses encoding the rat dominant-negative Akt (AdAktDN) were also prepared as described previously (33). In this adenovirus, both Thr308 and Ser473 of the rat Akt1 were replaced by alanine (33).

Induction of ARF

Male Sprague-Dawley rats (Saitama Experimental Animal Supply, Saitama, Japan) that weighed 150 to 200 g were anesthetized intraperitoneally with sodium pentobarbital (30 mg/kg) at surgery. The left renal artery was occluded with Sugita aneurysm clips (Mizuho Ikakogyo, Tokyo, Japan) for 60 min. The clamps were removed after 60 min; the incisions were closed; and the rats were killed at 0, 6, 12, 24, 48, and 72 h ($n = 5$). The left kidney was removed quickly and processed for histologic evaluation, protein extraction, or RNA extraction. Age- and weight-matched Sprague-Dawley rats also received sham operations in a similar manner, except for clamping of the renal arteries at 6, 12, and 24 h ($n = 5$).

Isolation of Kidney Tissue and Histologic Examination

Rats were anesthetized with pentobarbital at indicated times after the ischemic event. Their kidneys were perfused with sterile PBS. The left kidney was excised quickly, frozen in liquid nitrogen, and homogenized in the SDS sample buffer described later.

For immunohistochemical studies, renal tissues were fixed in formalin overnight and then dehydrated and embedded in paraffin. Thin sections were examined with periodic acid-Schiff staining as described previously (34). Immunohistochemical staining was performed by a streptavidin and biotin technique using an anti–Ets-1–specific antibody (Santa Cruz Biochemical; N-276, cs-111), anti–proliferating cell nuclear antigen (PCNA)-specific antibody (Santa Cruz Biochemical; PC-10, cs-56), and anti–aquaporin-1–specific antibody (Santa Cruz Biochemical; B-11, sc-25287) as markers for proximal tubules, as described previously (35–37).

Western Blot Analysis

Homogenized total renal tissue or LLC-PK1 cells were lysed in an SDS sample buffer (50 mM HEPES [pH 7.5], 150 mM NaCl, 1.5 mM $MgCl_2$, 1 mM EGTA, 10% glycerol, 1% Triton X-100, 1 μg/ml aprotinin, 1 μg/ml leupeptin, 1 mM PMSF, and 0.1 mM sodium orthovanadate) at 4°C (38). Protein was transferred to a nitrocellulose membrane and probed with the anti–Ets-1–specific antibody. The primary antibodies were detected using horseradish peroxidase–conjugated rabbit anti-mouse IgG and visualized by the Amersham ECL system (Amersham, Arlington Heights, IL).

Electrophoretic Mobility Shift Assay

Nuclear extracts from the renal cortex were prepared as described previously (39). The extracts (10 μg) underwent a reaction in a premixed incubation buffer (Gel Shift Assay Kit; Promega) with the γ-^{32}P-end-labeled ets-1 binding site of a cyclin D1 promoter-lesion (5'-GATCTCGAGCAGGAAGTTCGA-3') for 30 min at 25°C. To establish the specificity of the reaction, we performed competition

assays with 100-fold excess of unlabeled ets-1 binding oligonucleotides (heterologous competitor DNA). To perform supershift assay, we added 5 μg of anti–Ets-1 antibody (Santa Cruz; N-276, cs-111) to the nuclear extracts, incubated extracts for 1 h at 4°C, and performed gel shift assay. After the reaction, the samples were analyzed on a 6% nondenaturing polyacrylamide gel. The gel was dried, and the protein-DNA complexes were visualized by autoradiography.

Real-Time Quantitative PCR

We performed a reverse transcription–PCR (RT-PCR) reaction for Ets-1 from RNA extracted from the ischemia-reperfusion kidneys. Total RNA was harvested from renal tissue using TRI-REAGENT (Life Technologies) (40). One microgram of total RNA samples was used for the RT-PCR as follows. The real-time quantitative PCR method was used to detect accurately the changes in Ets-1 gene copies. Total RNA was harvested from renal tissue. Rat Ets-1 and glyceraldehyde-3-phosphate-dehydrogenase (GAPDH) mRNA were amplified. The primers for rat Ets-1 were 5'-GCCCAGCTTCATCACAGAGT-3' (upper) and 5'-TGTTGAAAGATGACTGGCTG-3' (lower) (23). The predominant cDNA amplification product was predicted to be 296 bp in length. The RT-PCR of GAPDH served as positive controls. The primers for rat GAPDH were 5'-TCCCTCAAGATTGTCAGCAA-3' (upper) and 5'-AGATCCACAACGGATACATT-3' (lower) (41). The predominant cDNA amplification product was predicted to be 309 bp in length. PCR products were detected and quantified in real time using the LightCycler Real-Time PCR (Roche Molecular Biochemicals, Tokyo, Japan) as described previously (42,43). A three-step PCR was performed for 35 cycles. Denaturation was performed at 94°C for 20 s, annealing at 55°C for 20 s, and extension at 72°C for 30 s. The PCR products of Ets-1 and GAPDH were subcloned to the TA cloning vector (Promega, Biotec, Madison, WI) as described previously (40). The plasmids that contained Ets-1 cDNA and GAPDH cDNA were used to make standard curves of quantitative PCR.

Cell Proliferation Analysis by [^{3}H]Thymidine Incorporation

After transfection, the LLC-PK1 cells were plated in 24-well plates and incubated in a medium without FCS for 20 h. For the last 4 h, the cells were pulsed with 1 μCi [^{3}H]thymidine (Amersham). After the incubation, the cells were redissolved in 0.5 M NaOH and counted in an Aquasol-2 scintillation cocktail (NEN Research Products, Boston, MA) (44).

Caspase 3 Assays

A Caspase 3 Fluorometric Protease Assay Kit (MBL, Tokyo, Japan) was used for the measurement of caspase 3 activities as described previously (33). In brief, the cells were plated in six-well dishes and infected with adenoviruses. The cell lysates then were incubated with the same amounts of reaction buffer and a 50-mM DEVD-AFC substrate for 2 h at 37°C. Fluorescence was monitored with an excitation wavelength of 400 nm and an emission wavelength of 505 nm.

Cell Death ELISA

Histone-associated DNA fragments were quantified by ELISA (Boehringer Mannheim). All cells from each well were collected by trypsinization and pipetting, then pelleted (800 rpm, 5 min), lysed, and subjected to ELISA capture according to the manufacturer's protocol (33). Cytosolic proteins were collected using a cell lysis buffer and centrifuged according to the manufacturer's protocol. The nucleus formed into a pellet, and the cytoplasmic fraction became the supernatant. These supernatants were collected for the ELISA assay. Each experiment was carried out in triplicate and repeated in at least five independent experiments.

Statistical Analyses

The results are given as means ± SEM. The differences were tested using a two-way ANOVA followed by the Scheffe test for multiple comparisons. Two groups were compared by the unpaired t test. $P < 0.05$ was considered significant.

Results

Western Blot Analysis of the Protein Expression of Ets-1 and HIF-1α after Ischemic Renal Failure

The left renal artery was clamped for 60 min and the left kidney was excised at 0, 6, 12, 24, 48, and 72 h after reperfusion. Western blot analysis was used to detect the protein levels of Ets-1 and actin. The expression of Ets-1 was weak in the control kidney (0 h) and sham-operated kidneys (6 and 12 h; Figure 1). The expression of Ets-1 was dramatically increased at 6 to 24 h after ischemia-reperfusion (Figure 1A). The upregulation of Ets-1 protein expression was temporary, with the intensity of the Ets-1 band decreasing at 48 and 72 h after ischemia-reperfusion. The protein levels of Ets-1 exhibited no changes after 6 to 12 h in the sham-operated rats (the data of 24 h are not shown). Western blot analysis was used to detect the protein levels of HIF-1α and actin. The expression of HIF-1α was weak in the control kidney (0 h) and sham-operated kidneys (6 and 12 h; Figure 1). The expression of HIF-1α was dramatically increased as early as 6 h after ischemia-reperfusion (Figure 1A). The upregulation of HIF-1α protein expression was temporary, with the intensity of the

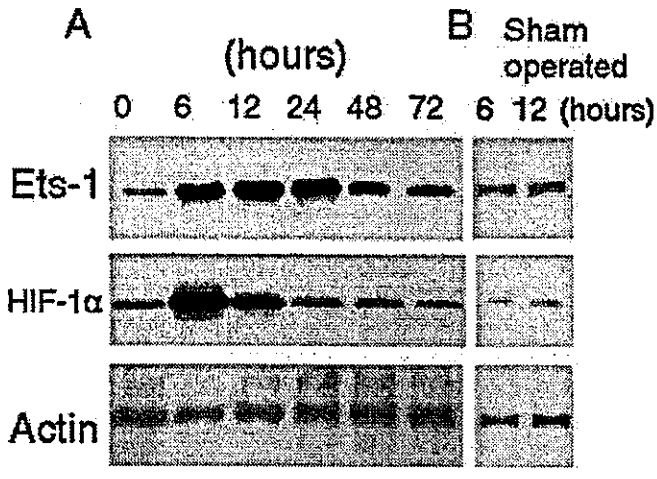

Figure 1. Protein expressions of Ets-1 and hypoxia-inducible factor-1α (HIF-1α) in the kidneys of rats that were subjected to 60 min of renal ischemia. The left renal artery was clamped for 60 min, and the left kidney was excised at 0, 6, 12, 24, 48, and 72 h after reperfusion (A). A sham operation was performed, and the left kidney was excised at 6 and 12 h (B). Extracted protein (20 μg) from renal tissue was separated by SDS-PAGE gels. Ets-1, HIF-1α, and actin protein levels were detected by Western blot analysis.

Ets-1 band decreasing at 48 and 72 h after ischemia-reperfusion. We performed an immunoblot for actin as a loading marker, and there were no significant changes in actin during ischemia-reperfusion. The protein levels of HIF-1α exhibited no changes after 6 to 12 h in the sham-operated rats (the data of 24 h are not shown).

Immunohistochemical Examination of Ets-1 in ARF

Next, we performed immunohistologic studies on Ets-1 in ARF (Figures 2 and 3). In a low-power view examination, Ets-1 expression was observed in cortical renal tubules at 12 h after ischemia-reperfusion (Figure 2A). We used the anti–aquaporin-1 antibody as a marker of proximal tubules (35–37). As shown in Figure 2, A and B, the expression of Ets-1 is co-localized with aquaporin-1 in the low-power view examination in continuous sections. Conversely, only a slight Ets-1 expression is observed in the renal cortex form control rats (Figure 2E), whereas the expression of aquaporin-1 is clearly observed in the renal cortex form control rats (Figure 2F). From these results, Ets-1 was expressed mainly in the proximal tubules of the renal cortex 12 h after ischemia-reperfusion (Figure 2). In the renal medulla, Ets-1 could not be detected in either the ischemia-reperfusion kidney (Figure 2C) or the control kidney (data not shown). In a higher-power view, Ets-1 staining was observed in the nucleus of proximal tubular cells (Figure 3A). As shown in Figure 3B, the expression of Ets-1 is co-localized with aquaporin-1 in continuous sections. To examine the specificity of the antibody, we used a blocking peptide (sc-111p; Santa Cruz Biotechnology). The nuclear signal diminished in the presence of the blocking peptide in the cortex of ischemia-reperfusion kidney (Figures 2G and 3C).

To co-localize Ets-1 with dividing cells, we examined Ets-1 staining at 24 h after ischemia-reperfusion (Figure 4). Ets-1 expression was observed at the proximal tubules of the cortex (Figure 4, A and C). PCNA staining was also observed at the proximal tubules of the cortex (Figure 4, B and D). The higher power view of Ets-1 staining also revealed co-localization of Ets-1 and PCNA in the same tubules at 24 h after ischemia-reperfusion in continuous sections (Figure 4, C and D). Conversely, only a slight Ets-1 expression is observed in the renal cortex from control rats (Figure 4E). No PCNA-positive tubules were observed from control rats (Figure 4F). To examine the specificity of the antibody, we used a blocking peptide (sc-9857p; Santa Cruz Biotechnology). The nuclear signal diminished in the presence of the blocking peptide in the cortex of ischemia-reperfusion kidney (Figure 4G).

Real-Time PCR

Quantification of the Ets-1 mRNA transcript using the real-time quantitative PCR method revealed 8.0-fold (6 h), 3.8-fold (12 h), and 2.2-fold (24 h) increases in Ets-1 mRNA levels compared with the 0-h value (Figure 5). The linear curve between the cDNA amount and PCR product was observed in the same range utilized by using the Ets-1 cDNA plasmid. The signals of Ets-1 were not significantly changed in the sham-operated rat kidneys. The GAPDH signal was not significantly changed by ischemia-reperfusion (Figure 5A).

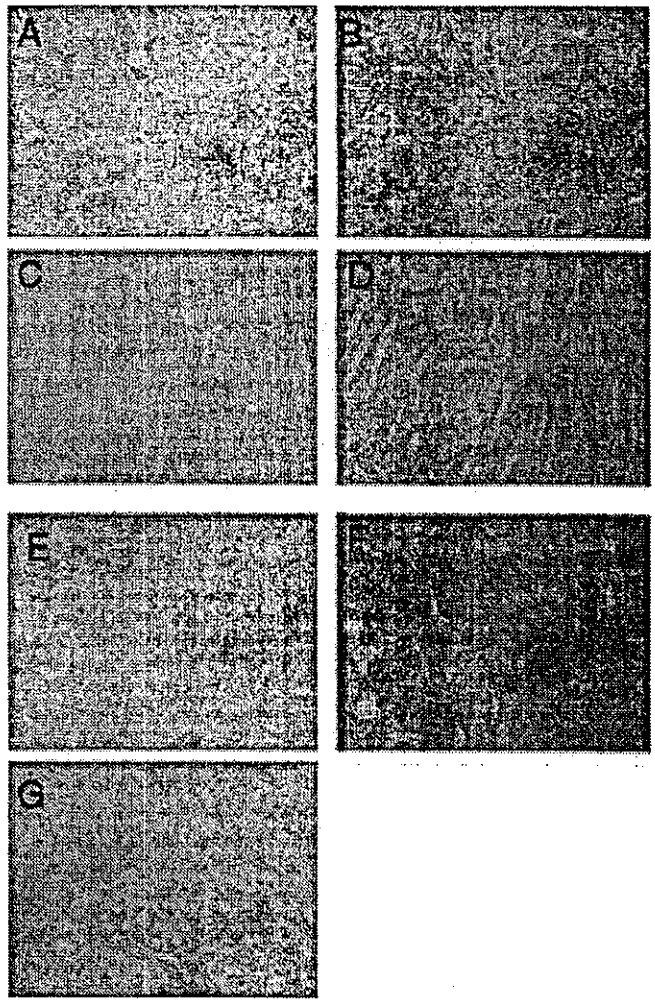

Figure 2. Immunohistological examination of Ets-1 in ischemic-reperfusion kidneys. Immunohistochemical analyses at a low-power view (×100) of the renal cortex were performed with antibodies against Ets-1 (A) and aquaporin-1 (B) at 12 h after ischemic injury. Immunohistochemical analyses at a low-power view (×100) of the renal medulla were performed with antibodies against Ets-1 (C) and aquaporin-1 (D) at 12 h after ischemic injury. Immunohistochemical analyses at a low-power view (×100) of the renal cortex of control kidneys were performed with antibodies against Ets-1 (E) and aquaporin-1 (F). Immunohistochemical analyses at a low-power view (×100) of the renal cortex of ischemic kidneys were performed with antibodies against Ets-1 in the presence of a blocking peptide (G). Histologic examinations A and B, C and D, and E and F are continuous sections, respectively.

Hypoxia Stimulates Ets-1 Expression and Promoter Activity via HIF-1α in LLC-PK1 Cells

To examine whether hypoxia-reperfusion stimulates Ets-1 expression and promoter activity in renal tubular cells, we used a hypoxic culture system with LLC-PK1 cells. We exposed LLC-PK1 cells to hypoxia for 3, 6, and 6 h + reoxygenation 6 h and examined the promoter activity of Ets-1 and the expression of Ets-1 protein by Western blot analysis. In the

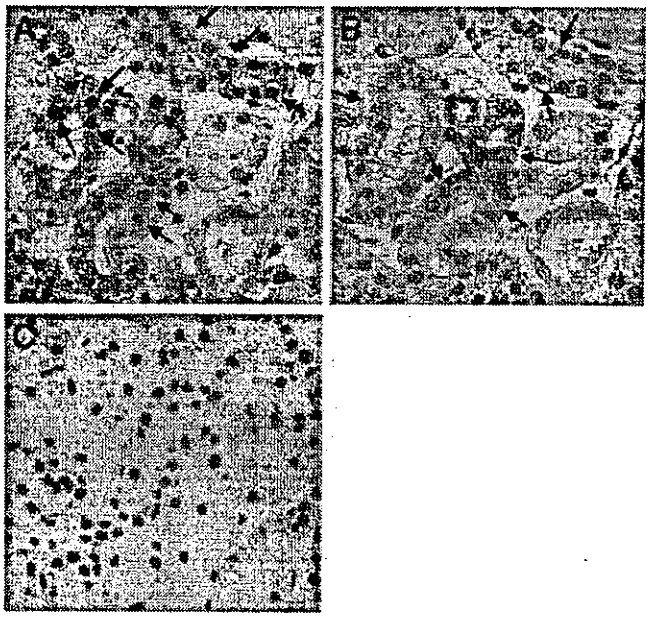

Figure 3. Immunohistologic examination of Ets-1 in proximal tubules of ischemic-reperfusion kidneys. Immunohistochemical analyses at a high-power view (×400) of the renal cortex were performed with antibodies against Ets-1 (A) and aquaporin-1 (B) at 12 h after ischemic injury. Histologic examinations A and B are continuous sections. The arrows indicate Ets-1– and aquaporin-1–positive cells. When a blocking peptide was added to the anti–Ets-1 antibody solution, no positive signal was observed in ischemia-reperfusion kidney (12 h; C).

promoter assay experiments, the Ets-1 promoter-luciferase plasmid was transfected in LLC-PK1 cells 48 h before hypoxia. As shown in Figure 6B, Ets-1 promoter activity was increased 7.1-fold at 3 h, 9.1-fold at 6 h, and 12.1-fold at 6 h + reoxygenation 6 h. Hypoxia also induced changes in the Ets-1 protein level in LLC-PK1 cells (Figure 6A). There were no significant changes in actin during hypoxia/reoxygenation.

To test whether the upregulation of Ets-1 is dependent of HIF-1α, we examined Ets-1 protein expression and promoter activity in HIF-1α–transfected LLC-PK1 cells and dnHIF-1α–transfected LLC-PK1 cells. The hypoxic inducibility of the Ets-1 promoter assay in HIF-1α–overexpressing and dnHIF-1α–overexpressing cells was 17.8- and 1.5-fold, respectively, as compared with 9.1-fold in control LLC-PK1 cells at 6 h (Figure 6D). The Western blot analysis demonstrated that transfection of dnHIF-1α reduced the increment of Ets-1 protein by hypoxia (Figure 6C). These results indicated that the upregulation of Ets-1 by hypoxia is dependent on HIF-1α.

Electrophoretic Mobility Shift Assay

To examine the induction of cyclin D1 expression *via* the ets-1 binding site, we performed an electrophoretic mobility shift assay using nuclear extracts from a rat renal cortex. Figure 7 shows that the nuclear extract from the ischemia-reperfusion rat renal cortex gave rise to a protein-DNA complex (Figure 7, lane 2). However, we did not detect protein-DNA complex

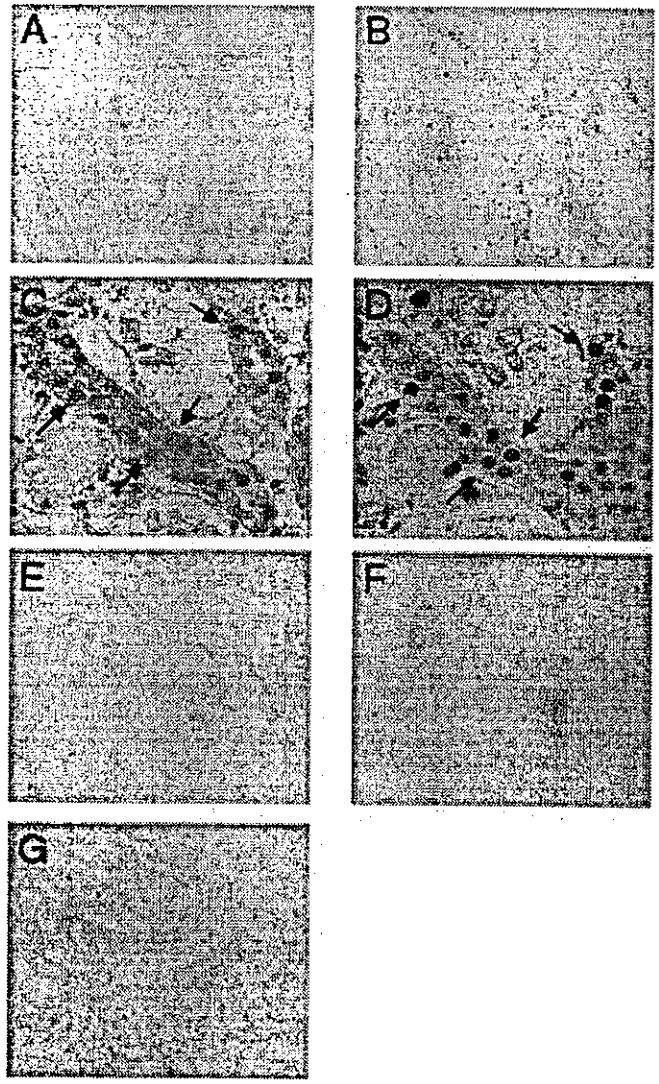

Figure 4. Immunohistologic co-localization of Ets-1 and proliferating cell nuclear antigen (PCNA) in the proximal tubules of ischemic-reperfusion kidneys. Immunohistochemical analyses at a low-power view (×100) of the renal cortex were performed with antibodies against Ets-1 (A) and PCNA (B) at 24 h after ischemic injury. Histologic examinations A and B are continuous sections. Immunohistochemical analyses at a high-power view (×400) of the renal cortex of ischemic kidneys were performed with antibodies against Ets-1 (C) and PCNA (D) at 24 h after ischemic injury. The arrows indicate Ets-1– and PCNA-positive cells. Immunohistochemical analyses at a low-power view (×100) of the renal cortex were performed with antibodies against Ets-1 (E) and PCNA (F) of control kidney. Histologic examinations E and F are continuous sections. When a blocking peptide was added to the anti-PCNA antibody solution, no positive signal was observed in ischemia-reperfusion kidney (12 h; G).

band in control rat renal cortex (Figure 7, lane 3). The band was completed using 100-fold excess of the unlabeled oligonucleotides (heterologous competitor DNA; Figure 7, lane 4). When nuclear extracts from the ischemia-reperfusion rat renal cortex were preincubated with anti–Ets-1 antibody, the super-

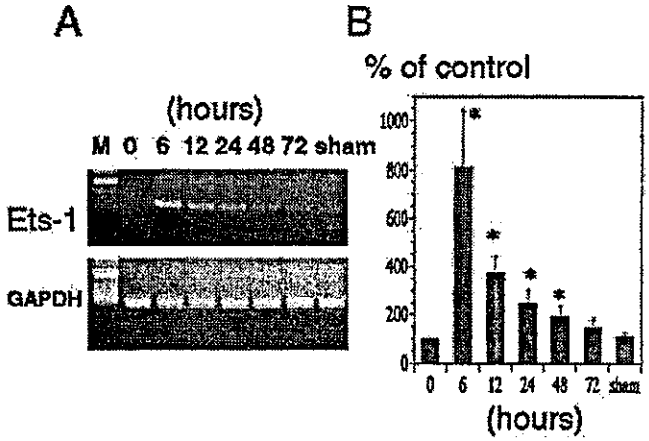

Figure 5. Quantitative analysis of Ets-1 expression in ischemic-reperfusion kidneys using real-time PCR. The left renal arteries were clamped for 60 min, and kidneys were excised at 0, 6, 12, 24, 48, and 72 h after reperfusion. Sham-operated rats at 6 h were also examined. Extracted total RNA were subjected to quantitative PCR using the LightCycler Real-Time PCR for the estimation of relative Ets-1 mRNA levels and the Ets-1 to glyceraldehyde-3-phosphate-dehydrogenase (GAPDH) mRNA ratio, as described in the Materials and Methods section. (A) The representative agarose gels for Ets-1 and GAPDH are shown. (B) Each column with a bar shows the mean ± SEM ($n = 5$). $^*P < 0.05$ *versus* control rats.

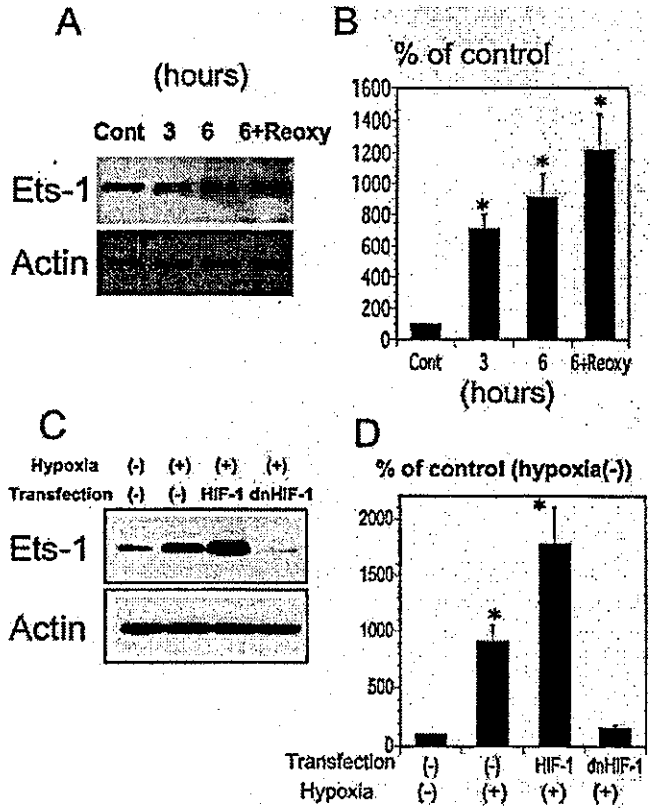

Figure 6. Hypoxia stimulates Ets-1 expression and promoter activity *via* HIF-1α in LLC-PK1 cells. To examine whether hypoxia/reoxygenation stimulates Ets-1 expression and promoter activity in renal tubular cells, we used a hypoxic culture system with LLC-PK1 cells. We exposed LLC-PK1 cells to hypoxia for 3, 6, and 6 h + reoxygenation 6 h and examined the promoter activity of Ets-1 and the expression of Ets-1 protein by Western blot analysis. (A) Hypoxia induced changes in the Ets-1 protein level in LLC-PK1 cells by Western blot analysis. (B) Ets-1 promoter activity was increased 7.1-fold at 3 h, 9.1-fold at 6 h, and 12.2-fold at 6 h + reoxygenation. (C and D) To test whether the upregulation of Ets-1 is dependent on HIF-1α, we examined Ets-1 protein expression and promoter activity in HIF-1α–transfected LLC-PK1 cells and dnHIF-1α–transfected LLC-PK1 cells; $n = 5$, mean ± SEM; $^*P < 0.05$ *versus* control.

shift of the band was observed (Figure 7, lane 6). These results confirm that Ets-1 binds to the ets-1 binding site of the cyclin D1 promoter in the ischemia-reperfusion condition.

Cell Proliferation and Cyclin D1 Expression by the Overexpression of Ets-1 in LLC-PK1 Cells

We first examined the effects of the overexpression of Ets-1, using an adenovirus, on the cell proliferation of LLC-PK1 cells by [^{3}H]thymidine uptake. Figure 8A shows the effects of Ets-1 on [^{3}H]thymidine uptake. Overexpression of Ets-1 stimulated the [^{3}H]thymidine uptake to 225% dose-dependently. Overexpression of Adnull (control adenovirus) did not significantly change the [^{3}H]thymidine uptake in LLC-PK1 cells. We next examined the role of Ets-1 in the regulation of cyclin D1 promoter activity and protein expression. We performed a transient transfection with the cyclin D1-luciferase reporter gene and the β-galactosidase expression vector and then infected it with Adets-1 or Adnull. When Ets-1 was overexpressed, cyclin D1 promoter activity increased significantly, by 3.6-fold, in LLC-PK1 cells. In the case of transfection of Adnull, there were no significant changes in cyclin D1 promoter activity or protein expression (Figure 8B). When Adets-1 was transfected, a higher level of cyclin D1 protein expression could be detected when compared with Adnull (Figure 8B).

Apoptotic Changes by the Overexpression of Ets-1 in LLC-PK1 Cells

In vascular endothelial cells, overexpression of Ets-1 causes apoptotic changes (30). Thus, we examined the effects of the overexpression of Ets-1 using an adenovirus on apoptotic changes of LLC-PK1 cells by caspase 3 activity and a cell death ELISA kit. We used AdAktDN as a positive control. Overexpression of AdAktDN caused apoptotic changes in renal tubular cells (33). Figure 9 shows the effects of Adets-1, AdAktDN, and Adnull on caspase 3 activity and the cell death ELISA. Overexpression of AdAktDN stimulated caspase 3 activity and the value of cell death ELISA. Overexpression of Adets-1 did not significantly change stimulated caspase 3 activity or the value of cell death ELISA in LLC-PK1 cells. These data demonstrated that Ets-1 does not cause apoptotic changes in LLC-PK1 cells.

Discussion

In the present study, we demonstrated that Ets-1 is upregulated in proximal tubules in the recovery phase of ARF, that